Structural and Mutational Analyses of *Aspergillus fumigatus* SidA: A Flavin-Dependent *N*-hydroxylating Enzyme

Michael Gerald Fedkenheuer

Thesis submitted to the faculty of

Virginia Polytechnic Institute and State University

In partial fulfillment of the requirements for the degree of

Master of Science in Life Sciences

In

Biochemistry

Pablo Sobrado

Carla V. Finkielstein

Bin Xu

July 27, 2012

Blacksburg, Virginia

Keywords: *Af* SidA, hydroxylation, *N*-hydroxylating Monooxygenases, flavin, siderophore

Structural and Mutational Analysis of *Aspergillus fumigatus* SidA: A Flavin-Dependent *N*-hydroxylating Enzyme

Michael Gerald Fedkenheuer

Pablo Sobrado, Chair

Department of Biochemistry

ABSTRACT

SidA from *Aspergillus fumigatus* is an *N*-hydroxylating monooxygenase that catalyzes the committed step in siderophore biosynthesis. This gene is essential for virulence making it an excellent drug target. In order to design an inhibitor against SidA a greater understanding of the mechanism and structure is needed. We have determined the crystal structure of SidA in complex with $NADP^+$, Ornithine, and FAD at 1.9 Å resolution. The crystal structure has provided insight into substrate and coenzyme selectivity as well as residues essential for catalysis. In particular, we have chosen to study the interactions of Arg 279, shown to interact with the 2'phosphate of the adenine moiety of $NADP^+$ as well as the adenine ring itself. The mutation of this residue to alanine makes the enzyme have little to no selectivity between coenzymes NADPH and NADH which supports the importance of the ionic interaction between Arg279 and the 2'phosphate. Additionally, the mutant enzyme is significantly more uncoupled than WT enzyme with NADPH. We see that the interactions of the guanadinyl group of Arg279 and the adenine ring are also important because K_M and K_d values for the mutant enzyme are shifted well above those of wild type with coenzyme NADH. The data is further supported by studies on the reductive and oxidative half reactions. We have also explored the allosteric effect of L-arginine. We provide evidence that an enzyme/coenzyme/L-arginine complex is formed which improves coupling, oxygen reactivity, and reduction in SidA; however more work is needed to fully understand the role of L-arginine as an allosteric effector.

ACKNOWLEDGMENTS

I would like to thank my advisor Dr. Pablo Sobrado for his guidance and support. His critical reasoning ability and attention to detail has been invaluable during my time in his laboratory. Additionally, I am very grateful to my graduate committee for their critical analysis of my research and input into important experiments that I needed to accomplish. I would also like to thank all the members of the Sobrado lab for their support and knowledge that has helped me through my graduate career. I would like to thank Dr. Andrea Mattevi and Stefano Franceschini for solving the crystal structure of SidA. I would like to thank the NSF for funding this research, and finally I would like to thank my family and my brother for their continued support during my experiences at Virginia Tech.

Table of Contents

LIST OF FIGURES

Chapter I

Chapter III

LIST OF TABLES

Chapter III

CHAPTER I

Introduction

Aspergillus fumigatus is the most common causal agent of fatal invasive mycoses and is the cause of 90% of systemic, invasive aspergillosis (IA) in its respective genus [1, 2]. *A. fumigatus* establishes an opportunistic infection and is only virulent in the respiratory tract of immune-compromised individual [1, 2]. This fungus produces large quantities of robust airborne spores which are abundant in soil and decaying matter. *A. fumigatus* is ubiquitous in the air, and each day humans inhale several hundred conidia [2]. A healthy immune system is capable of clearing these spores through pulmonary defense mechanisms. However, in immune-compromised individuals, the conidia are able to develop into mycoses [1].

In addition to IA, exposure to *A. fumigatus* can cause atopic asthma, aspergilloma, hypersensitivity pneumonitis, asthma, chronic obstructive respiratory disease, and allergic broncho-pulmonary aspergillosis (ABPA) in asthma and cystic fibrosis (CF) patients [3]. ABPA progression can be problematic for individuals with CF, leading to severe bronchitis and pulmonary hypertension [3, 4]. The current treatments for an *A. fumigatus* infection include prednisone, inhaled corticosteroids, itraconzole, voricoazole, and azithromycin. These treatments are classified as steroids, antibiotics, and antifungal agents but are vastly ineffective at clearing an infection [5]. Additionally, toxicity issues associated with almost all of these drugs makes long term usage impossible, especially for treating immune compromised individuals [5]. Due to these problems, a safe and effective *A. fumigatus* treatment is needed.

Due to the severe nature of an *A. fumigatus* infection, there has been a concerted effort to determine virulence factors associated with this fungus [1]. One strategy for mammalian cells to

inhibit growth of microbial pathogens is to sequester iron [6, 7]. In humans, serum iron concentrations are approximately 10^{-24} M. Most microorganisms require an iron concentrations roughly equal to 10^{-6} M to survive [6]. Thus, these organisms rely on either reductive iron uptake or siderophore-mediated iron uptake. *A. fumigatus* relies solely on siderophore-mediated iron uptake through four known siderophores: fusaricine C, triacetylfusaricine, ferricrocin, and ferrichrome [1]. Siderophores bind iron with an extremely high affinity and can be used for iron storage and transport. It has been shown that iron is essential for the formation and maturation of the conidiophore [8].

Whole genome sequencing of *A. fumigatus* has spurred efforts to determine the effect of genes related to siderophore biosynthesis (SB). Many *A. fumigatus* SB mutations confer variations in virulence. Perhaps the most interesting candidate was the gene denoted SidA. SidA catalyzes the first step in SB, and a ΔsidA strain of *A. fumigatus* was unable to produce an infection in an IA mouse model [1].

SidA from *A. fumigatus* is an *N*-hydroxylating flavin containing monooxygenase (NMO) that catalyzes the conversion of L-ornithine to N^5-hydroxyornithine using the co-enzyme NADPH and molecular oxygen. Additionally, SidA can utilize the coenzyme, NADH but with roughly 10 fold less efficiency [9]. The product of this reaction is then incorporated into the backbone of the hydroxamate-based siderophore, ferrichrome, which binds Fe^{3+} with a high affinity (Figure 1.1) [6]. SidA is essential for infection and there are no homologues in humans, which make it an excellent drug target [9].

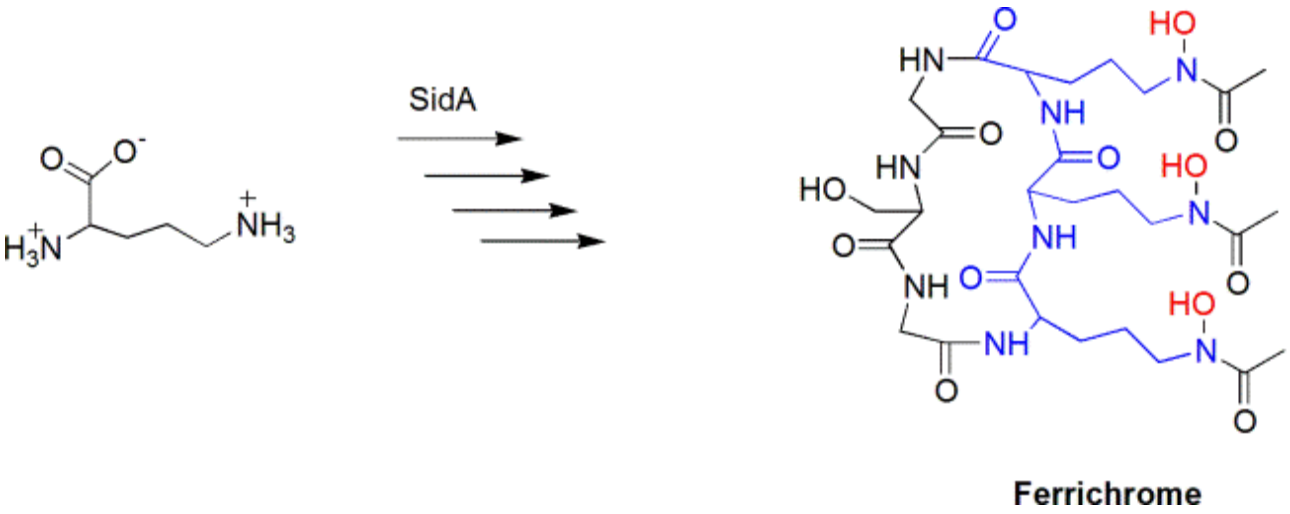

Figure 1.1. SidA catalyzes the committed step in siderophore biosynthesis by generating N^5-hydroxy ornithine. The ornithine is shown in blue, while the N^5-hydroxyl group is shown in red in the completed siderophore.

A mechanism of *Af* SidA has been proposed and tested by our lab and is consistent with that of other flavin containing monooxygenases. The first step in catalysis is reduction of the oxidized flavin by NADPH, which transfers the R-hydride [10]. This leaves the oxidized coenzyme ($NADP^+$), which remains bound for the remainder of the catalytic cycle. In the next step of the reaction, the flavin can react with molecular oxygen creating a peroxyflavin at the C4a position of the flavin. This intermediate is rapidly protonated to yield a stable C4a-hydroperoxyflavin intermediate which is stabilized by the oxidized coenzyme. A molecule of L-ornithine can then be hydroxylated by the C4a-hydroperoxyflavin yielding N^5-hydroxyornithine and a hydroxyflavin. The product is released along with a water molecule leading to a dehydrate flavin. The flavin then returns to the oxidized state after release of $NADP^+$ from the active site (Figure 1.2) [9].

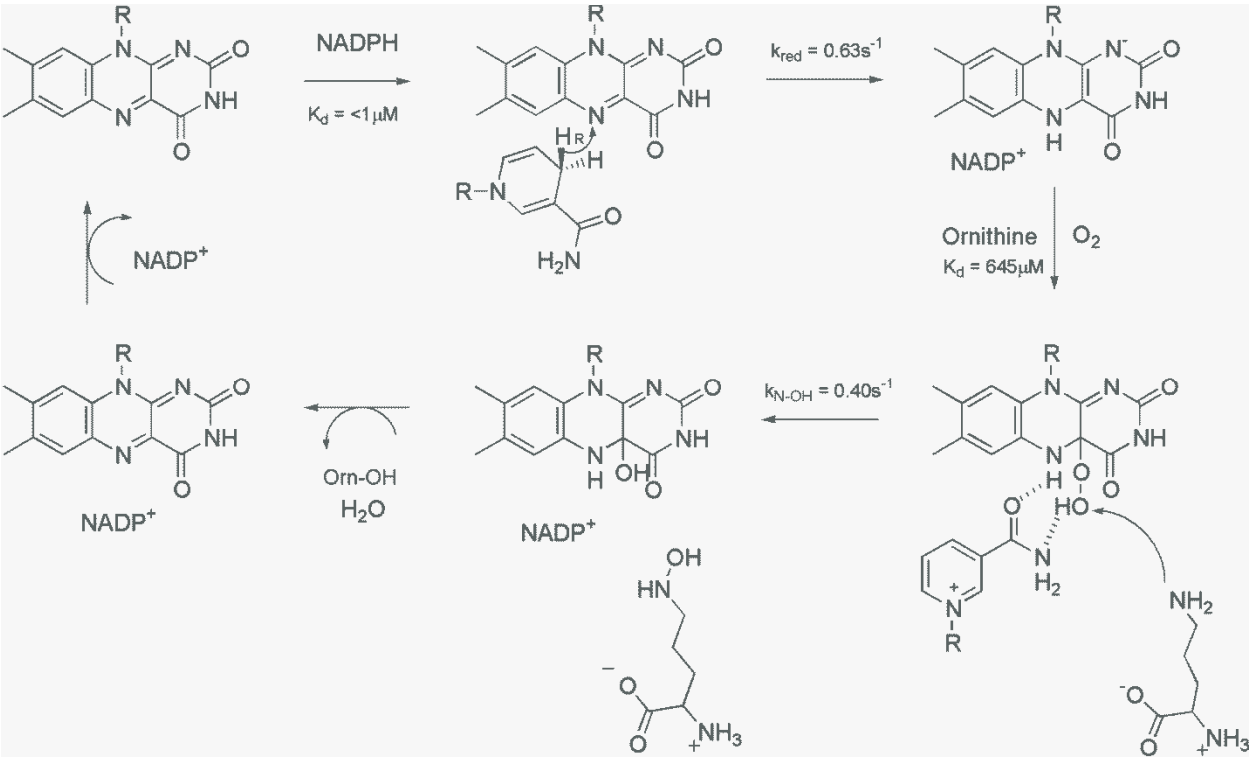

Figure 1.2. The catalytic cycle of SidA begins with reduction of the flavin by NADPH. $NADP^+$ remains bound through the catalytic cycle to stabilize the N^5 of the flavin and the C4a-hydroperoxyflavin which is generated through reaction with molecular oxygen. The C4a-hydroperoxyflavin intermediate can then hydroxylate a molecule of L-ornithine. The catalytic cycle is completed by re-oxidation of the flavin.

This thesis will address the structure of SidA as determined by x-ray crystallography. Additionally, we present mutational analysis of residue Arg279 which we have shown to be critical in catalysis and coenzyme selectivity. Kinetic comparisons between the wild type (WT) and mutant enzyme show the critical nature of interactions with the 2'phosphate of the adenine moeity of NADPH as well as the equally important interactions with the adenine ring itself. Recent data has suggested that L-arginine is an allosteric activator of SidA; however a detailed kinetic analysis has yet to be completed. In this thesis we present evidence that L-arginine siginficantly improves product formation by increasing the rate of the reductive half reaction and acts to improve the formation and stability of the critical C4a-hydroperoxyflavin intermediate in the oxidative half reaction. Future work needs to be done to crystalize SidA in the absence of coenzyme in order to understand molecular motion of this enzyme.

CHAPTER II

Materials and Methods

Protein Expression

Recombinant SidA was subcloned into pET-15b vector (Novagen). In this plasmid, full length protein is expressed with an N-terminus 6xHis fusion. The plasmid was transformed into BL21(DE3)pLysS-T1^{R} *Escherichia coli* cells (Sigma Chemical Co.) and expression was performed using auto-induction media. In general, 6 L of media were grown at 37 °C for ~ 7 h followed by overnight incubation at 25 °C and yielded ~ 90 g of cells. The cell pellet was frozen at -80°C.

Purification of SidA 6xHis-tag fusion

Ninety grams of cell paste were resuspended in 300 mL buffer A (25 mM HEPES, 300 mM NaCl, 20 mM immidazole pH 7.5). The resuspended solution was then incubated with 25 μg/mL lysozyme, DNase I, and RNAse for 45 min at 4 °C with constant stirring. The resulting solution was then sonicated on ice for 5 min at 70 % amplitude with 15 s of sonication and 10 s of rest time. The lysate was then centrigued at 10,000 xg for 45 min. After this time, the supernatant was collected and loaded onto three in tandem pre-equilibrated (Buffer A) 5mL His•Trap columns via an FPLC system. After loading was completed, the columns were washed with buffer A until the A_{280} returned to baseline levels. The columns were then washed with Buffer B (25 mM HEPES, 300 mM NaCl, and 120 mM immidazole pH 7.5) to remove contaminants. SidA was then eluted with Buffer C (25 mM HEPES, 300 mM NaCl, and 300 mM immidazole pH 7.5). Purified SidA was then buffer exchanged into Buffer D (100 mM Sodium Phosphate and 50 mM NaCl pH7.5) via a series of concentration/dilution steps. The enzyme was frozen in

30 μL drops in liquid nitrogen at a final concentration of 300 μM. The yields were an average of 25 mg pure protein per liter of culture.

Purification of SidA for Crystallization

Purification of SidA for crystallization was done exactly as mentioned above; however, once the protein had eluted from the column, the buffer was exchanged into Buffer E (25 mM HEPES, 300 mM NaCl pH 7.5). The purified protein was then incubated with thrombin 2 mg/mL overnight at 4 °C with stirring to remove the His-tag. The solution was then passed back over the Ni^{2+} resin. SidA has an affinity for the Ni^{2+} resin which allowed us to remove the thrombin protease without an additional purification step. After the columns were washed with Buffer E and the A_{280} returned to baseline, the cleaved SidA was eluted with 30 mM immidazole. SidA that was uncleaved eluted at 300 mM immidazole. The fraction that eluted at 30 mM immidazole was buffer exchanged into Buffer F (25 mM HEPES, 100 mM NaCl pH 7.5). This fraction was concentrated to 100 μM and frozen at -80 °C in 150 μL aliquots.

Determination of Flavin Incorporation

Flavin incroporation was determined by mesuring protein concentration using the bradford assay and comparing that to protein concentration measured by flavin absorbance. Determining protein concentration based on absorbance was done by using the extiniction coeficent 13.7 $mM^{-1}cm^{1}$ at 450 nm. Flavin incorporation was generally 70%.

Site Directed Mutagenesis

Site directed mutagenesis of SidA was performed using the QuikChange protocol (Agilent Technologies), using the forward primer (5'-

GCACCACCCTGATCATGGCCGACTCGGCTATGCGCCC-3') and reverse primer (5'-GGGCGCATAGCCGAGTCGGCCATGATCAGGGTGGTGC-3'). The modified codon to yield R279A is shown in bold letters.

Crystallization

Af SidA crystals containing only $NADP^+$ or $NADP^+$ and either L-ornithine, L-arginine, or L-lysine were obtained using the hanging drop vapor diffusion method (conditions: 1.6 M ammonium sulfate, 0.1 M HEPES Sodium (pH 6.6), 2% dioxane). A solution of 8 mg/ml SidA was incubated with $NADP^+$ (1 mM) and L-ornithine (15 mM), L-arginine (15 mM), or L-lysine (15 mM) for 1 h at 4 °C. Protein and well solution were mixed at a ratio of 1:1 to a final volume of 1 μL l per droplet. 4 droplets were prepared over a final well volume of 200 μL, yielding prism-like yellow crystals that grew in 3-4 days at room temperature.

Preparation of Crystals for Data Collection

Oxidized SidA crystals were transferred to a 1 μL solution containing 2 M ammonium sulfate, 4% dioxane, 0.1 M HEPES, and 20% glycerol at pH 7.5. Crystals were flash frozen in liquid nitrogen.

Preparation of reduced crystals

Oxidized SidA crystals were transferred to a 1 μL solution containing 2 M ammonium sulfate, 4% dioxane, 0.1 M HEPES, 20% glycerol, and either 1 mM NADPH or saturated with dithionite at pH 7.5. Crystals were flash frozen in liquid nitrogen after bleaching of the yellow color, consistent with reduction was observed.

Oxygen consumption assay

The amount of molecular oxygen consumed by *Af* SidA was monitored using a Hansatech Oxygraph system (Norfolk, England). Each assay was performed in 1 mL, 100 mM sodium phosphate, pH 7.5, at 25 °C. When the rate of oxygen consumption was measure as a function NADPH concentrations (0.005-1 mM), the concentration of L-ornithine was at 10 mM. In assays that were performed varying L-ornithine, L-lysine, or L-ornithine, NADPH concentrations were kept constant at 1 mM. The effect of arginine was measured by determining the activity of *Af* SidA in the presence of 10 mM ornithine, 1 mM NAPDH at various concentrations of arginine (not shown). It was determined that at 1 mM arginine the increase in the activity was maximized. The oxidase activity was measured in the presence of 1 mM NADPH in the absence of hydroxylable substrate. In all of the assays, the reaction was initiated by the addition of 2 μM *Af* SidA and monitored for 5 min with constant stirring.

All data was fit using the Michaelis Menten Equation where k_{cat} is the maximum reaction rate and K_M is the kinetic binding value.

$$\boldsymbol{v} = \frac{\boldsymbol{kcat}\,[\boldsymbol{S}]}{\boldsymbol{Km} + [\boldsymbol{S}]}$$

N5-hydroxyornithine detection assay

The amount of hydroxylated product formed by *Af* SidA was measured using a variation of the Csaky iodine oxidation reaction described in Robinson et al [11]. The standard assay buffer contained 104 μL of 100 mM sodium phosphate (pH 7.5) and concentrations of L-ornithine and NAD(P)H ranging from 0 to 20 mM and from 0 to 6 mM respectively. In assays that were performed with varying amounts of L-ornithine, NADPH concentrations were kept constant at 1 mM. In assays that were performed with varying amounts of NADPH, L-ornithine concentrations

were kept constant at 10 mM. Saturating concentrations of L-arginine for WT and mutant enzymes were by the oxygen consumption assay. In assays done to measure the effect of L-arginine, NADPH was varied as mentioned above while L-ornithine was kept at 10 mM. Reactions were initiated by addition of *Af* SidA (2.0 μM), and the reaction was allowed to proceed for 10 min at 25 °C with shaking at 750 rpm.

N-5 hydroxyornithine formation data was fit to a product inhibition formula, where k_{cat} is the maximum rate of the reaction, K_M is the observed kinetic binding, and K_i is the inhibition:

$$\boldsymbol{v} = \frac{\boldsymbol{kcat}[\boldsymbol{S}]}{\boldsymbol{Km} + [\boldsymbol{S}] + (\frac{[\boldsymbol{S}]^2}{\boldsymbol{Ki}})}$$

Flavin Fluorescence Assay

The flavin fluorescence was measured at 15 μM enzyme concentration in a total volume of 100 μL (100 mM Sodium Phosphate pH 7.5). Increasing $NADP^+$ concentrations were added from 0-1 mM for WT SidA and 0-6 mM for mutant proteins. Increasing NAD^+ concentrations were added from 0-5 mM for WT and mutant proteins. Solutions were incubated for 5 min in 98 well black corning plates and excited at 450 nm. Emission was measured between 500 and 625 nm with a 495 nm cut-off filter.

The following equation was used to fit data from the fluorescence assay, where F_{NOX} refers to the fluorescence value at each oxidized nucleotide concentration $[N_{OX}]$

$$\boldsymbol{F} = \frac{\boldsymbol{F_{NOX}}[\boldsymbol{N_{OX}}]}{\boldsymbol{K_d} + [\boldsymbol{N_{OX}}]}$$

Rapid Reaction Kinetics: Reductive Half Reaction

Anaerobic reduction of SidA was carried out using single-mixing mode of an SX20 stopped-flow apparatus (Applied Photophysics, UK). 30 μM enzyme was mixed with an equal volume of NADPH ranging from 0-1 mM for WT enzyme and 0-5 mM for mutant enzyme. When using NADH the concentrations ranged from 0-5 mM for WT and mutant enzymes. The reaction proceeded at 15°C until full flavin reduction was observed. Flavin reduction was monitored by reduction of the absorbance at 452 nm. The observed rate constants were determined by plotting the data using KaleidaGraph (Synergy Software, Reading, PA).

The following equation was used to fit data from the reductive half reaction, where k_{red} is the maximum rate of flavin reduction and K_d is the dissociation constant:

$$\boldsymbol{k_{obs} = \frac{k_{red}[S]}{K_d + [S]}}$$

Rapid Reaction Kinetics: Oxidative Half Reaction

The oxidative half reaction was carried out at 15 °C using the double-mixing mode of an SX20 stopped-flow apparatus (Applied Photophysics, UK) in an anaerobic glove box. Preparation of anaerobic buffer was carried about by repeated cycles of vacuum and flushing with O_2 free argon for 5 hours. The same procedure was used to make the enzyme anaerobic; however it was cycled for 2 hours. Anaerobic SidA at 60 μM was mixed with an equal volume of 60 μM [NADPH] for a final enzyme and coenzyme concentration of 30 μM. An initial test was done to determine the time scale for full reduction of the flavin, which was used as the lag time before mixing with buffer containing 200 μM O_2. The final concentration after double mixing was 15 μM. Re-oxidation of the flavin was measured by an increase in absorbance at 452

nm, and the production of the C4a-hydroperoxyflavin intermediate was measured by an increase in absorbance at 380 nm.

When the data were fit to a single exponential the following equation was used, where A is the absorbance at 380 or 452 nm, k_{obs} is the observed rate constant, and B_1 is the amplitude:

$$\boldsymbol{A = B_1 e^{(-k_{obs} t\ )}}$$

When the data were fit to a double exponential the following equation was used, where A is the absorbance at 380 or 452 nm, k_{obs1} and k_{obs2} are the apparent first order rate constants for the observed phases. B_1 and B_2 are the amplitudes of the corresponding phases while C is the final absorbance:

$$\boldsymbol{A = B_1 e^{(-k_{obs} t\ )} + B_2 e^{(-k_{obs} t\ )} + C}$$

CHAPTER III

Results and Discussion

a. Determination and Analysis of SidA Structure by X-ray crystallography

The crystal structure of SidA in complex with $NADP^+$ and L-ornithine was solved at 1.9 Å resolution. The crystal belonged to the space group I centered orthorhombic (I222), meaning 90 ° of data collection was sufficient to obtain a complete data set. The complete list of crystallographic parameter data can be found in Table 3.1. The phasing was solved by molecular replacement using L-ornithine hydroxylase from *Pseudomonas aeruginosa* (PvdA) as a template. SidA is organized as a tetramer with each subunit containing a bound FAD, $NADP^+$, and L-ornithine molecule (Figure 3.1). The $NADP^+$ molecule is positioned with the nicotinimide ring in close proximity to the N^5 and C4a positions of the flavin. The bound ornithine molecule is located adjacent to the flavin, poised to interact with the C4a-hydroperoxyflavin intermediate. The structure revealed that the $NADP^+$ and FAD molecules were each bound by an atypical Rossmann fold (3.1a). A Rossmann fold is a nucleotide binding domain commonly organized as a beta/alpha/beta motif. A typical Rossmann fold is comprised of 5 parallel beta strands linked to 3 anti-parallel beta strands by 2 alpha helices.

A

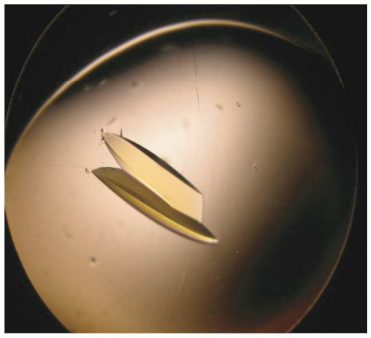

B

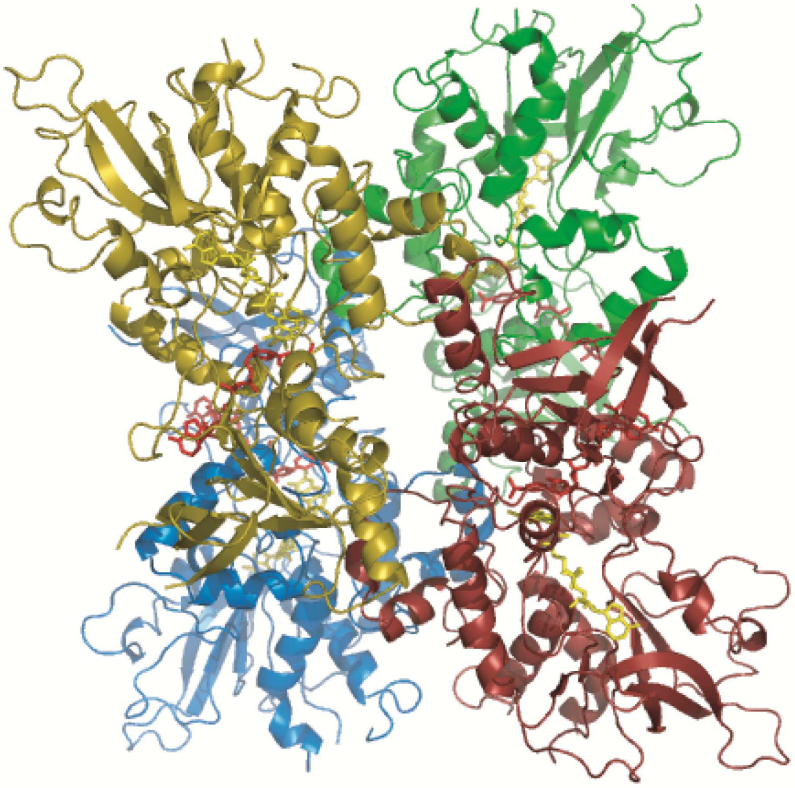

Figure 3.1. SidA is a tetramer determined by x-ray crystallography. Panel A shows a SidA crystal used for crystallography (size: 0.4 micron x 0.2 micron). Panel B shows the structure of SidA as a tetramer with each subunit in a different color. The bound FAD and $NADP^+$ molecules are depicted as sticks in yellow and red respectively.

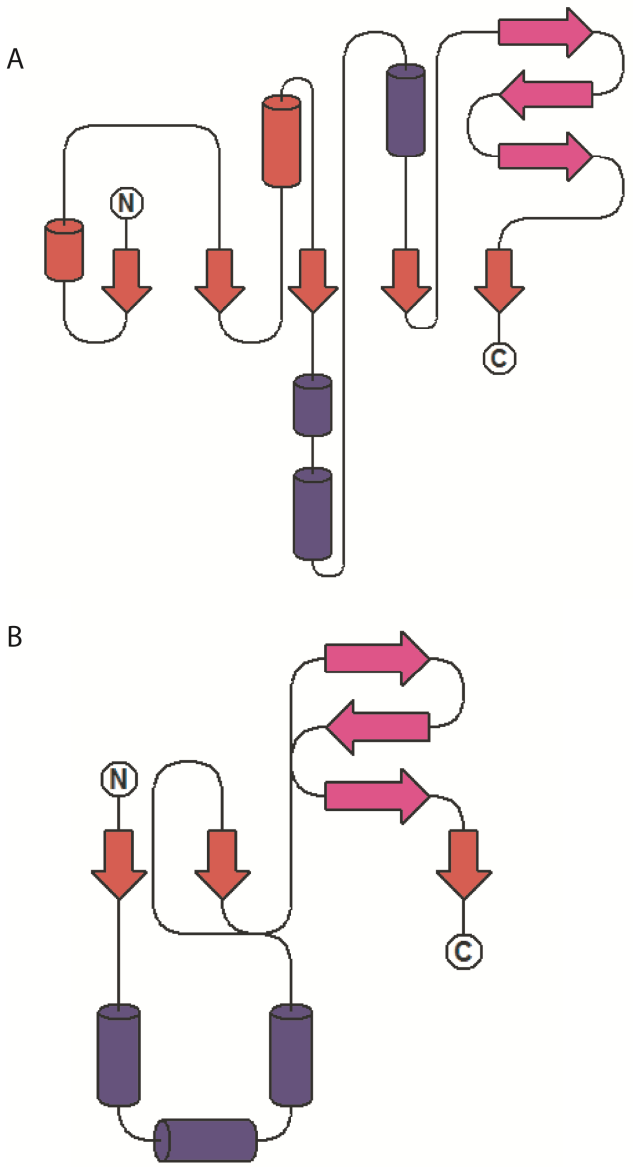

Figure 3.1a. SidA contains 2 Rossmann folds. The layout is depicted using a 2D topology map. Each Rossman fold binds either A) $NADP^+$ B) FAD where the alpha/beta/alpha motif is shown in red/blue/pink. In panel A, the additionall helicies which were not part of the Rossmann fold were left in red. The relative length of the alpha helicies and beta strands is crudely depicted, where alpha helicies and beta strand ≥ 6 amino acids are shown larger than those < 6 amino acids.

Table 3.1. The X-ray crystallographic parameters for the highest resolution crystal with $NADP^+$ and L-ornithine bound are shown here.

Crystallographic Parameter	Data
Unit cell (a,b,c) (Å)	77.80, 84.42, 145.13
Space group	I 2 2 2
Resolution (Å)	1.90
R_{merge} (%)	7.7 (50.7)
Completeness (%)	98.7 (99.5)
Unique reflections	38112
Redundancy	13.8 (13.0)
I/σ	12.1 (5.1)
No. of atoms	4023
Average B value ($Å^2$)	27.8
R_{cryst} (%)	20.41
R_{free} (%)	22.94
RMS bond length (Å)	0.0051
RMS bond angles (°)	0.999

*Highest resolution shells are shown in parenthesis

As shown in Figure 3.2, each SidA monomer is organized into 3 domains. The FAD binding domain is the largest, and is composed of residues 1-214, 409-456, and 466-501. The $NADP^+$ binding domain is composed of 215-285 and 325-408. The smallest domain is the L-ornithine binding domain contains residues 286-324 and 457-465.

The active site of SidA is arranged with the flavin extending into the center of the protein monomer with the isoalloxazine ring facing the nicotinimide ring of $NADP^+$ which extends into the active site from the opposite direction. As mentioned before, L-ornithine is bound between the $NADP^+$ and FAD molecules extending toward the C4a position of the flavin. It appears from the structure that the oxygen that is part of the amide group of the nicotinamide ring is capable of hydrogen bonding with the N^5 position on the flavin. It is also possible that the amino group can participate in hydrogen bonding with the C4a-hydroperoxyflavin intermediate (Figure 3.3).

Figure 3.3 specifically highlights residues that interact with $NADP^+$ and L-ornithine, as well as some residues speculated to be involved in catalysis. It appears that Lys105, Asn293, and Ser469 interact with the amino and carboxyl groups of ornithine. It is also possible that Asp288 plays a role in binding ornithine as well. Ser257 interacts with the 5'phosphate group of $NADP^+$, while Glu260, Arg144, Gln256, and Gln102 are positioned around the nicotinamide ring. It is important to note that the backbone nitrogen of Gln256 interacts with the 5' phosphate of $NADP^+$ as well through a helix dipole effect which creates a partial positive charge on this atom. This will be discussed in more detail later in the discussion.

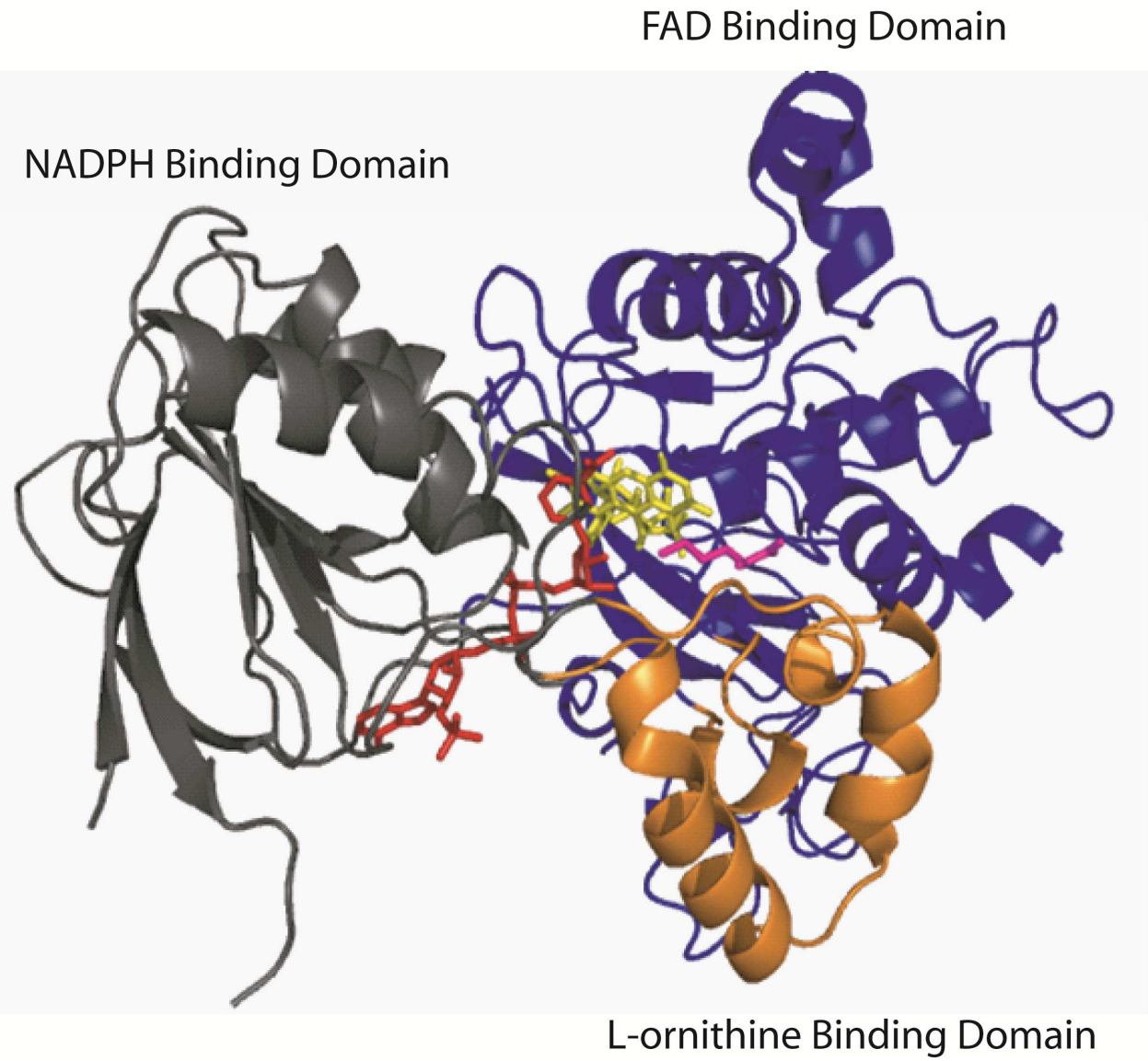

Figure 3.2. SidA is organized into three domains. SidA is displayed as a monomer with the flavin binding domain shown in blue, the NADP(H) binding domain in grey and the L-ornithine binding domain shown in orange. As sticks, the $NADP^+$ molecule is shown in red, the flavin is shown in yellow, and the ornithine molecule is shown in pink.

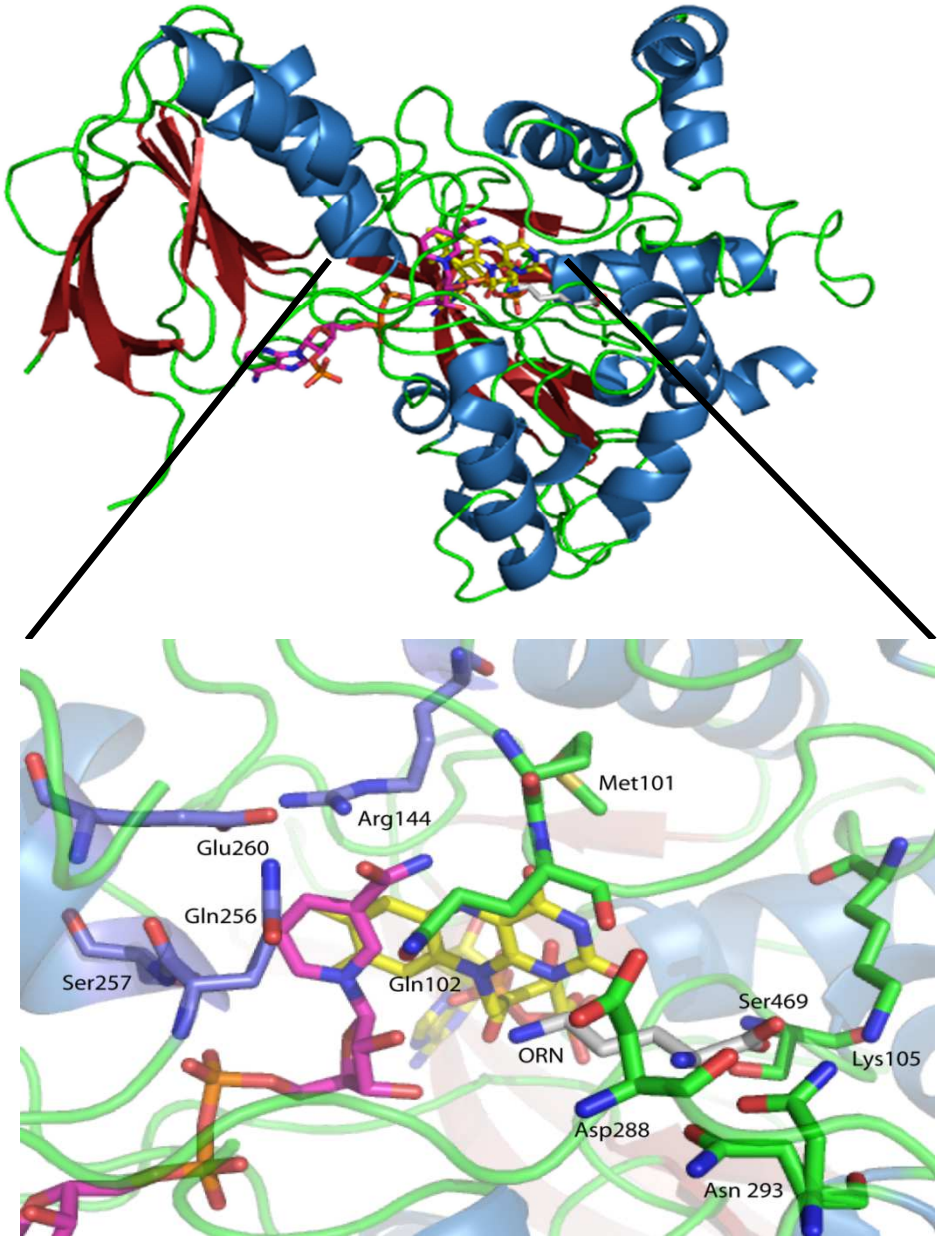

Figure 3.3. The SidA active site contains many several residues important for catalysis which are highlighted here. The top panel shows an individual SidA subunit with alpha helices in skyblue, beta sheets in firebrick, and loops in green. The bottom panel shows a blow up of the active site with $NADP^+$ and ornithine bound near the FAD cofactor. Residues that appear to bind ornithine and $NADP^+$ as well as possible catalytic residues are shown as sticks and are colored based on what secondary structure are contained in.

As previously mentioned, SidA is organized as a tetramer. Through analysis of the crystal structure, we were able to determine several motifs that involved in interactions between subunits. The largest motif is a helix loop helix motif between residues 281-294. This motif interacts with an identical motif from another subunit in the reverse orientation. For simplicity, each monomer will be referred to as M1-4, with M1 being the reference subunit. The interaction previously described was between M1 and M2. M1 and M3 are linked by 2 helix/helix interactions between residues 130-136 and 336-344. Residues 130-136 on M1 interact with residues 336-344 on M3 and vice versa. There are very few interactions between M1 and M4; however of particular note is ring stacking between phenylalanine 140 of each subunit (Figure 3.4).

It was of particular to interest to examine the interactions of SidA with $NADP^+$ and to understand the role of this coenzyme in oxygen activation. We have shown that SidA has a ten fold higher affinity for NADPH over NADH and maximum stability of the C4a-hydroperoxyflavin can only be achieved when using the coenzyme NADPH. It has been shown that when the enzyme is reduced with NADH, the hydroxylation reaction is uncoupled, leading to the release of the toxic reactive oxygen species, H_2O_2 [Pages 33-38]. Thus, by examining residues that interact with $NADP^+$ we were able to identify a residue, Arg279 that interacts with the adenine ring of $NADP^+$ and with the 2'phosphate group (specific to $NADP^+$) shown in Figure 3.5.

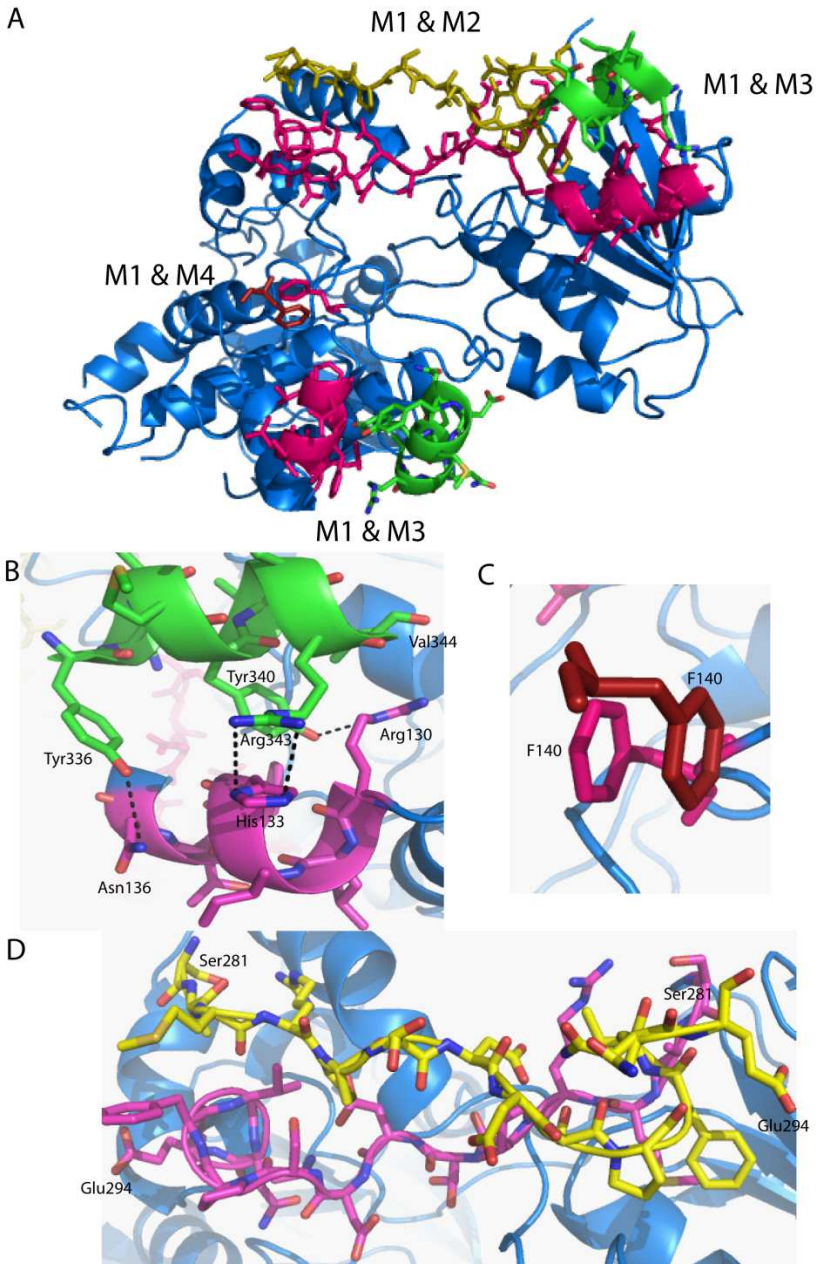

Figure 3.4. The interactions of each SidA subunit are shown here. Panel A shows a broad view of the interactions, where M1 is shown in blue with interacting domains shown in pink with sticks. Interacting residues of M2, M3, and M4 are shown in yellow, green, and red respectively. Panel B) shows detailed interaction between M1 and M3 C) shows detailed interactions between M1 and M4 D) depicts the interactions between M1 and M2. Residues at the start and end of an interaction region are labeled as well as those residues making key interactions.

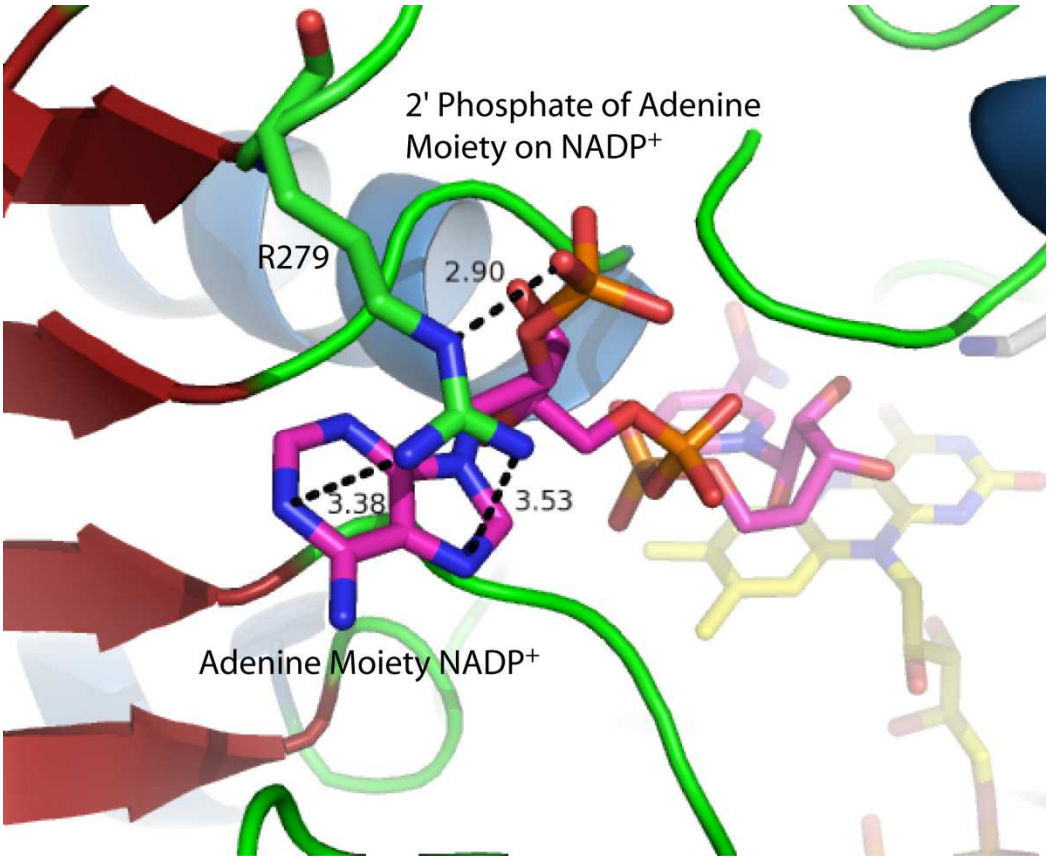

Figure 3.5: Arg279 interacts with the 2' phosphate of the ribose that carries the adenine moiety on $NADP^+$ as well as with the adenine ring. Alpha helicies, beta strands, and loops are shown in skyblue, firebrick, and green respectively. When shown as sticks, nitrogen atoms are blue, oxygen atoms are red, and carbons are depicted in pink, yellow, and green for $NADP^+$, FAD, and Arg279. Distances between atoms were determined using pymol v0.99.

Another residue of particular interest is Ser257. This residue appears to interact most likely through hydrogen bonding with the 5'phosphate group on $NAD(P)^+$. We speculated that this residue was involved in stabilizing the $NAD(P)^+$ positioning it to interact favorably with the flavin to promote oxygen reactivity and intermediate stability. Additionally, a helix dipole effect is observed with the 5'phosphate group, where the backbone nitrogen between Ser257 and Gln256 exhibits a partial positive charge that interacts with the negatively charged phosphate group (Figure 3.6).

The crystal structure of SidA was also solved in complex with L-lysine and in the absence of substrate. L-lysine is identical to L-ornithine but extends one methylene unit longer. Additionally, SidA hydroxylates lysine poorly and causes significant uncoupling of the reaction. In both crystal structures, no conformational changes were observed. The structure of SidA in complex with lysine was interesting, because it showed displacement of a water molecule originally observed between the L-ornithine molecule and the C4a-position of the flavin (Figure 3.7). This observation allowed us to speculate that SidA controls substrate selectivity through distance to the C4a-hydroperoxyflavin.

Reduced crystals that diffracted to 2.5 Å were produced by soaking oxidize SidA crystals in a solution of dithionite or NADPH. Bleaching of the crystals was observed in 5-10 s and re-oxidation (clear → yellow) took place rapidly (1-5 min) when dithionite was used and slowly (>1 hour) when NADPH was used as a reducing agent. Crystals that were reduced with both chemicals showed hydroxylated product bound in the active site, indicating that SidA is active in crystal form. Other than the presence of L-ornithine-OH, no significant conformational changes were observed between the oxidized and reduced structures.

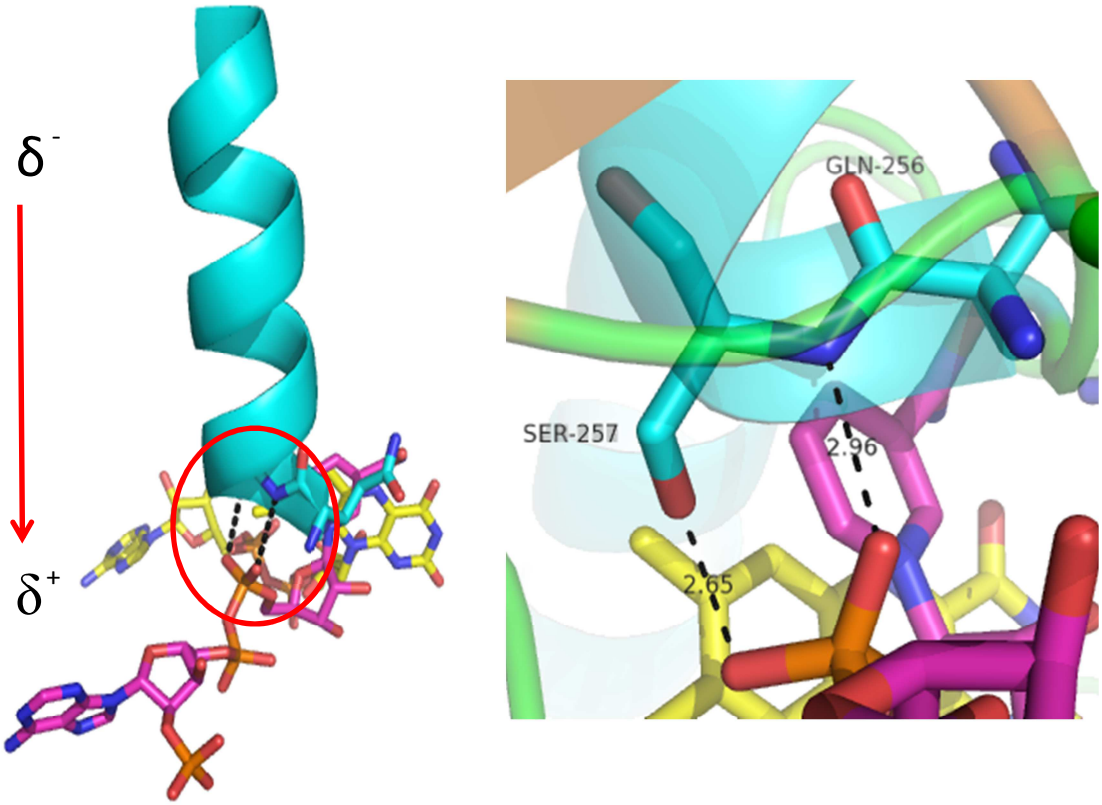

Figure 3.6. Residues Ser257 and Gln256 interact with the 2' phosphate of $NADP^+$. The left panel shows the helix containing Ser257 and Gln256 as well as the $NADP^+$ and FAD molecules. The partial positive charge at the N-terminal of the helix allows the backbone nitrogen of Gln256 to form and ionic interaction with the 5' phosphate $NADP^+$ (2.96 Å). The 5' phosphate interacts with the side chain of Ser257 through possible hydrogen bonding.

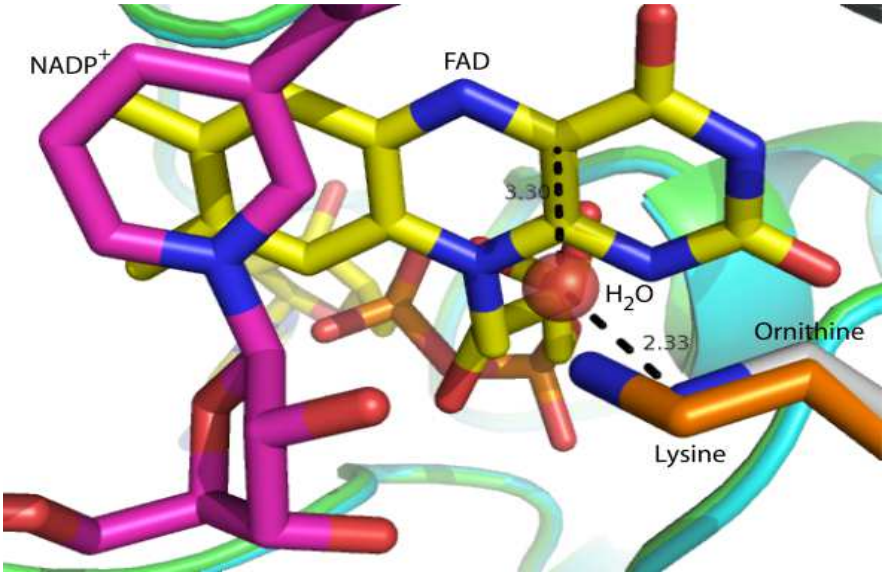

Figure 3.7. The crystal structure with L-ornithine bound versus that with L-lysine bound is depicted in this figure. The crystal structure with L-ornithine is shown in green while the crystal structure with L-lysine is shown in teal. The water molecule is shown in red as a sphere located within 2.33 Å of the N^5 position of the L-ornithine molecule and 3.30 Å from the C4a position of the flavin. The crystal structure with L-lysine bound does not contain a water molecule in this position.

b. Kinetic characterization of Arg279A mutant

As mentioned before, residue Arg279 was idenitifed through analysis of the crystal structure and appears to be important because it interacts with the adenine ring as well as the 2'phosphate on $NADP^+$. We speculated that this interaction is critical for the enzyme's specificity for NADPH over NADH. Additionally, we speculated that the interactions with the adenine moeity is important in binding affinity for both coenzymes. In order to test this hypothesis, site directed mutagenesis was used to replace the arginine at position 279 with an alanine. We will refer to this mutant enzyme as the R279A.

The wild type enzyme binds NADPH tightly with a measurable K_M of 7 μM while showing a roughly 10 fold decrease in the K_M for NADH measured to be 75 μM. In contrast, R279A binds NADPH loosely, showing a 40 fold increase in K_M (310 μM). As expected there is less of an effect (5 fold increase in the K_M) when using NADH (Table 3.2). The k_{cat} of the reaction is unchanged between mutant and WT enzyme. These data suggest that this mutation causes the enzyme to be ineffective in binding the 2' phosphate due to the observed lack of specificity for coenzymes. The increases in K_M values above those of WT with NADH are likely due to interactions of this residue with the adenine moiety (Figure 3.8).

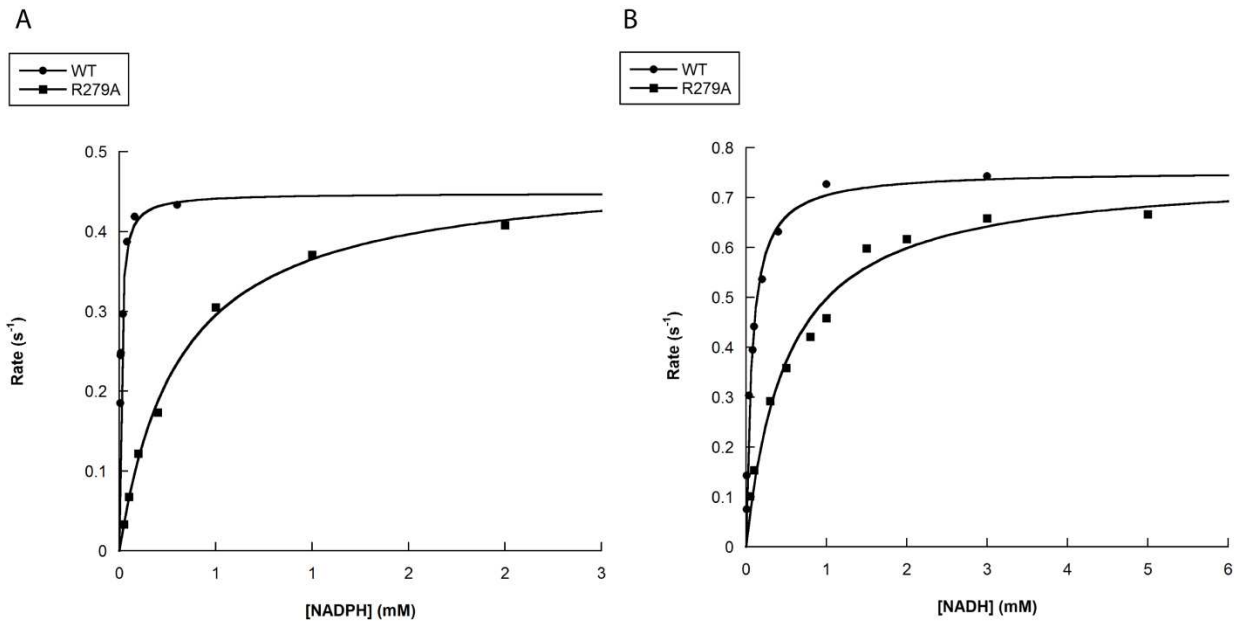

Figure 3.8. The oxygen consumption plots are shown for WT and R279A. Each assay was done at 15 mM L-ornithine and 2 μM final enzyme concentration in a 1 mL total reaction volume with varying concentrations of A) NADPH B) NADH.

Table 3.2. The values of oxygen consumption for WT and R279A are shown with varying concentrations NADPH and NADH. The percent coupling of the reaction is also shown.

	WT			**R279A**		
Enzyme	k_{cat} (s^{-1})	K_M (μM)	% Coupling	k_{cat} (s^{-1})	K_M (μM)	% Coupling
NADPH	0.45 ± 0.01	8 ± 1	92	0.48 ± 0.01	310 ± 24	50
NADH	0.75 ± 0.01	75 ± 7	53	0.75 ± 0.04	511 ± 71	33

To further understand this interaction, WT and R279A were compared in terms of product formation using the iodine oxidation assay. This assay allows us to follow product formation directly by measuring the amount of hydroxylamine produced in a reaction. The most notable change that was observed by studying product formation was that the mutant enzyme showed a 2 fold decrease in product formation when compared to WT enzyme (Figure 3.9, Table 3.3). The decreased k_{cat} observed for product formation did not match k_{cat} values obtained in the oxygen consumption assay suggesting that the reaction is uncoupled leading to the production of H_2O_2. It is likely that in addition to donating a hydrogen bond to the 2' phosphate, Arg279 is in fact interacting with the adenine moiety, stabilizing the $NADP^+$ molecule. This interaction appears to affects the stability of the intermediate which is supported by the increased uncoupling seen in the R279A mutant. The uncoupling observed in the R279A mutant is 50% with NADPH whereas there is only slight uncoupling observed with the WT enzyme. The R279A mutant is only 33% coupled with NADH while the WT enzyme with NADH is about 53% coupled.

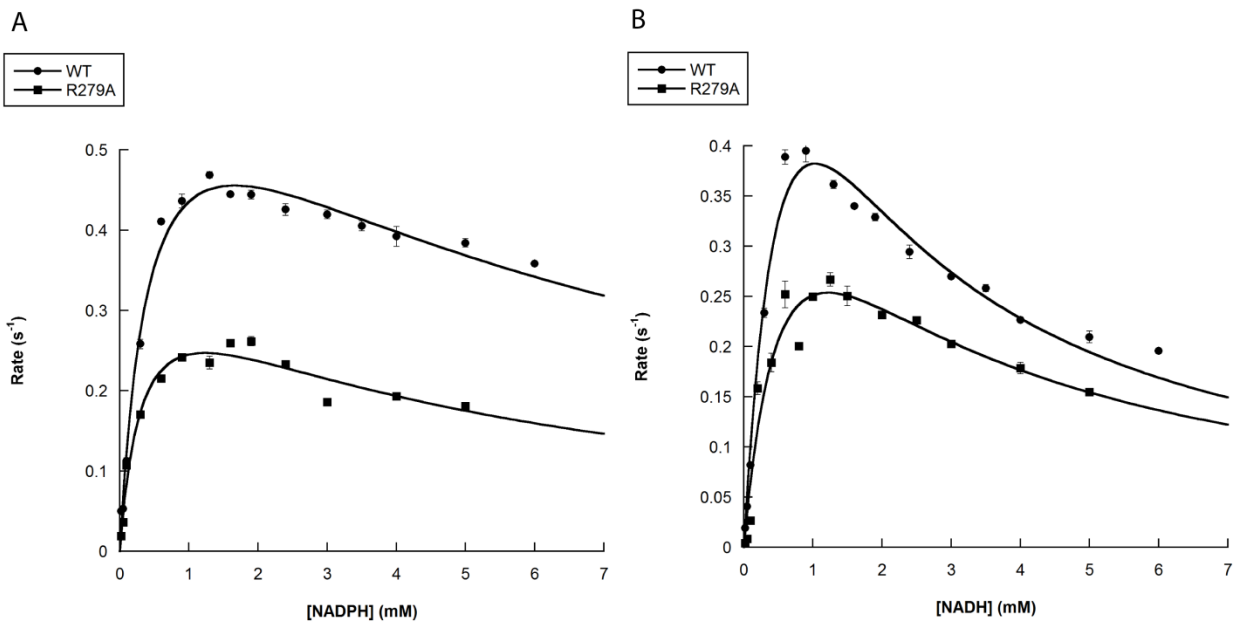

Figure 3.9. The *N*-5 hydroxyornithine detection plots are shown for WT and R279A. Each assay was done in triplicate at 15 mM L-ornithine at 2 μM final enzyme concentration in a total volume of 104 μL with varying A) NADPH B) NADH.

Table 3.3. The values of N^5-hydroxyornithine formation with varying NADPH and NADH for WT and R279A are shown here.

	NADPH			NADH		
Enzyme	k_{cat} (s^{-1})	K_M (mM)	K_i (mM)	k_{cat} (s^{-1})	K_M (mM)	K_i (mM)
WT	0.7 ± 0.05	0.45 ± 0.07	6.1 ± 1.1	1.0 ± 0.2	0.8 ± 0.2	1.2 ± 0.3
R279A	0.4 ± 0.05	0.35 ± 0.10	4.5 ± 1.5	0.5 ± 0.1	0.8 ± 0.3	2 ± 1

In order to probe the hypothesis that binding of the 2'phosphate by Arg279 is directly involved in inducing a conformational change favorable for C4a-hydroperoxyflavin intermediate stabilization the flavin fluorescence assay was used. The flavin can be excited at 450 nm and emits with a maximum value of 525 nm. Fluorescence increases as the microenvironment around the flavin becomes more hydrophobic, while a shift to a more hydrophilic environment would cause quenching. Thus, by adding coenzyme in various concentrations we can measure K_D values for the oxidized coenzymes and the particular changes they induce on the flavin. WT enzyme exhibits a profile where NAD^+ causes an increase in fluorescence while $NADP^+$ causes a decrease in fluorescence (Figure 3.10). We believe that the observed quenching is due to the nicotinimide ring being in close contact with the flavin, while the increase in fluorescence with NAD^+ is due to the flavin moving to a more hydrophobic environment but not being in close contact with the nicotinimide ring. Thus it appears the close proximity of the nicotinimide to the flavin is important for enhanced stability of the C4a-hydroperoxyflavin intermediate.

R279A exhibits an increase in fluorescence with both $NADP^+$ and NAD^+ which strongly suggests that this enzyme is functioning without coenzyme specificity (Figure 3.10). Additionally, a K_D for $NADP^+$ with WT was measured to be 18 μM while a K_d for $NADP^+$ with R279A was measured to be 725 μM (Table 3.4). This 40 fold increase in binding is consistent with values obtained from the oxygen consumption assay.

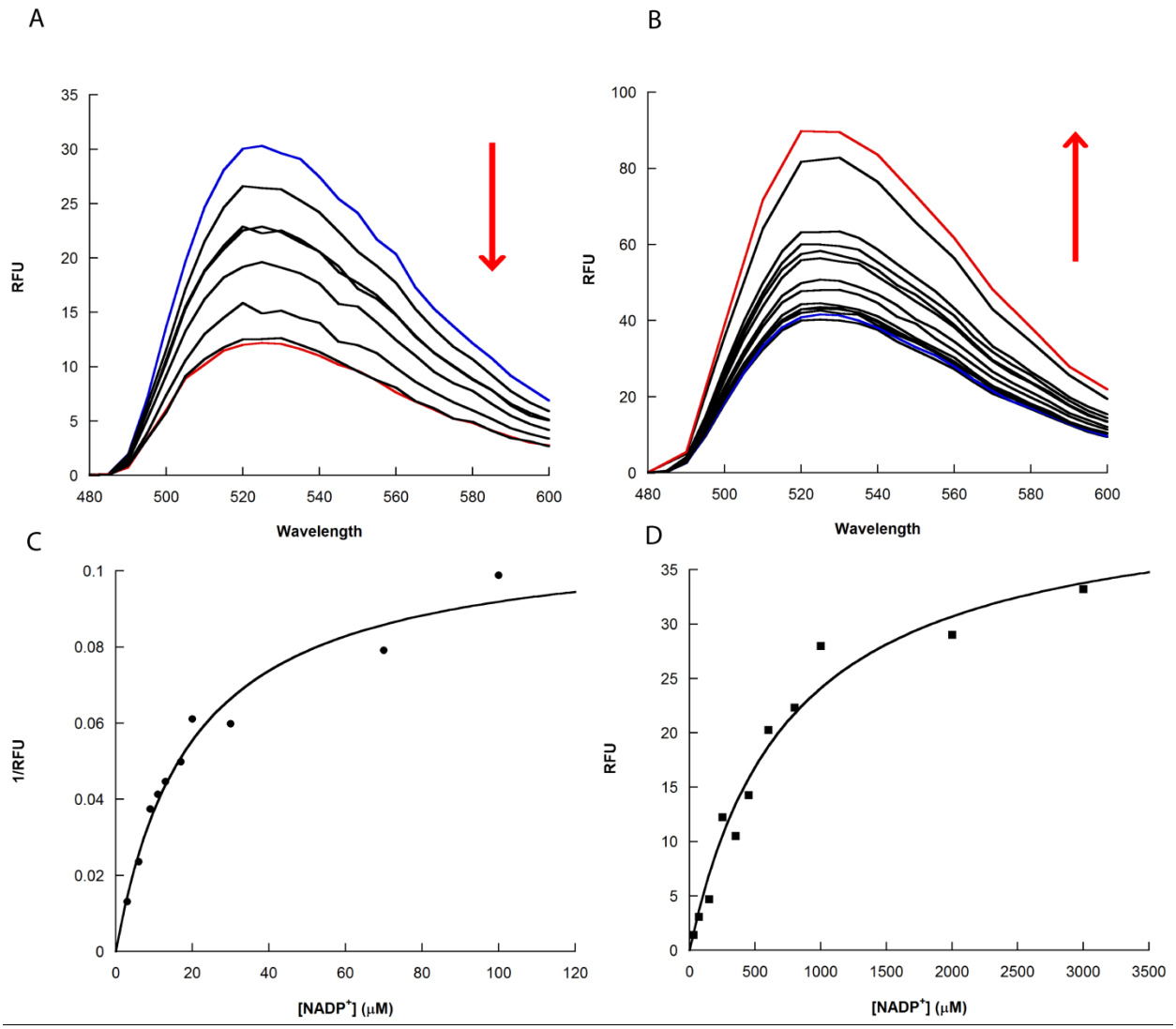

Figure 3.10. Fluorescence changes occur for WT and R279A with the addition of coenzyme. Panel A) shows the fluorescence trace for WT with $NADP^+$ while panel B) shows the fluorescence trace for R279A with $NADP^+$. Panel C) monitors the fluorescence changes at 525 nm for WT and panel D) monitors fluorescence changes at 525 nm for R279A. In panels A and B, the blue line represents the fluorescence with no coenzyme added and the red line represents the fluorescence at maximum coenzyme concentration (The red arrow indicates the shift in fluorescence with increasing [coenzyme]).

Table 3.4. The binding coefficients were measured by plotting fluorescence changes at 525 nm.

	$NADP^+$	**NAD^+**
Enzyme	K_d (μM)	K_d (μM)
WT	10 ± 1.1	252 ± 34
R279A	751 ± 140	380 ± 71

Rapid reaction kinetics following the reductive half reaction show an increase in K_d values for NADPH in the R279A mutant consistent with that observed in the steady state oxygen consumption assay (Figure 3.11, Table 3.5). Additionally, the K_d values were higher than those with WT enzyme with NADH suggesting the importance of the interaction with the adenine moiety. These data were consistent with the values obtained from the steady state oxygen consumption assay.

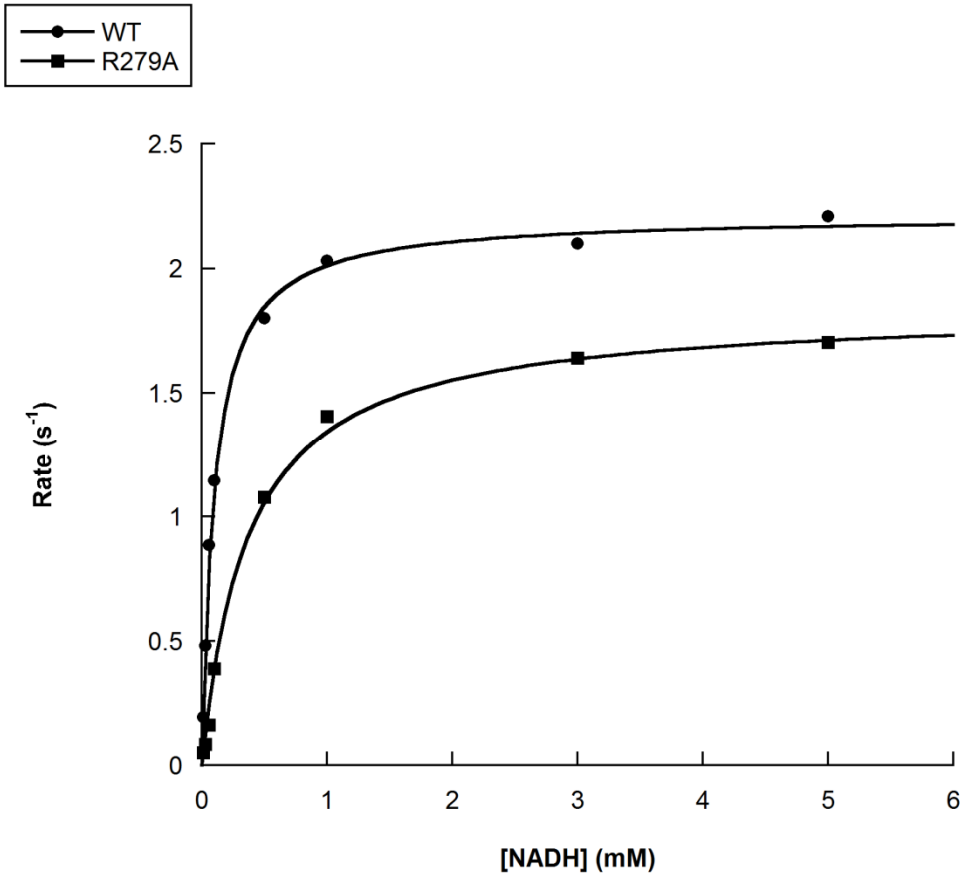

Figure 3.11. The reductive half reaction is depicted for WT and R279A with NADH. These data were obtained by measuring rates of anaerobic reduction in absorbance at 452 nm with increasing concentrations of NADH. Data was fit using a single exponential and these values were plotted versus concentration and fit with the Michaelis Menten Equation.

Table 3.5. The values for the reductive half reaction for WT and R279A with NADPH and NADH are shown here.

	NADPH		**NADH**	
Enzyme	k_{red} (s^{-1})	K_d (μM)	k_{red} (s^{-1})	K_d (μM)
WT	0.63	<1	2.2 ± 0.04	99 ± 7
R279A	0.879 ± 0.09	268 ± 92	1.84 ± 0.04	369 ± 34

The oxidative half reaction for WT enzyme showed formation of the C4a-hydroperoxyflavin as measured by A_{380} occurring at a $0.22s^{-1}$ with a decay of this intermediate denoted by $k2_{FADOOH}$ occurring at a rate of $0.005s^{-1}$. The re-oxidation of the flavin as measured by A_{452} took place in two phases as well. The first phase, $k1_{OX}$ was fast with a measured rate of $0.158s^{-1}$ while the second phase $k2_{OX}$ was slow with a measured rate of $0.008s^{-1}$ (Figure 3.12, Table 3.6). We hypothesize that the first rate corresponds to the formation of the C4a-hydroperoxyflavin because it is very similar to $k1_{FADOOH}$, while the second corresponds to the slow decay of this intermediate. These phases are poorly defined when NADH was used to reduce the enzyme indicating reduced stability of the C4a-hydroperoxyflavin which is consistent with the uncoupling observed with this coenzyme.

The oxidative half reaction for R279A was significantly different from WT. The profile showed a similar $k1_{FADOOH}$; however there was no observable decay at A_{380} of the intermediate indicating that decay and formation most likely took place simultaneously. Additionally, instead of measuring a negative absorbance for $k1_{OX}$, the R279A mutant had a rapid increase in absorbance at 452 nm, $0.816s^{-1}$ with NADPH and $0.443s^{-1}$ with NADH (Table 3.7). This phase was followed by a $k2_{OX}$ that matched the WT enzyme (Figure 3.13). These data strongly suggest that the mutant enzyme is unable to form a stable C4a-hydroperoxyflavin intermediate, and that it is formed and broken down rapidly. This is consistent with the reduced amounts of hydroxylated product formed by the mutant enzyme.

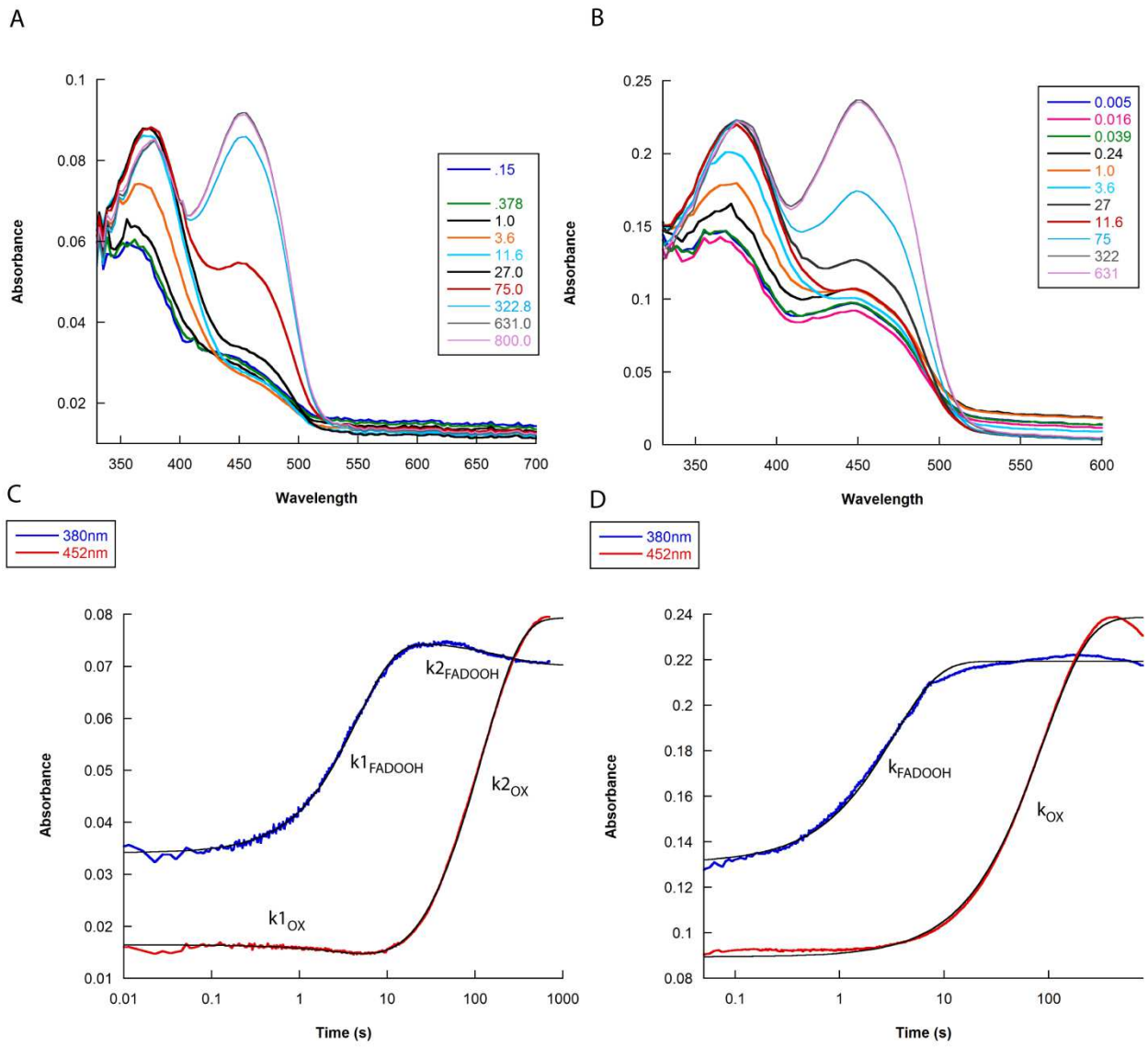

Figure 3.12. The oxidative half reaction was measured for WT enzyme. The top panels are traces of the oxidative half reaction for WT enzyme at various time points with A) NADPH and B) NADH. The bottom panels follow the absorbance at 380 nm (blue) and 452 nm (red) with C) NADPH and D) NADH. The fits shown in panels C and D are outlined by a thin black line and were fit to either single or double exponential growth or decay. The X axis is displayed in the logarithmic time scale to more clearly visualize the data.

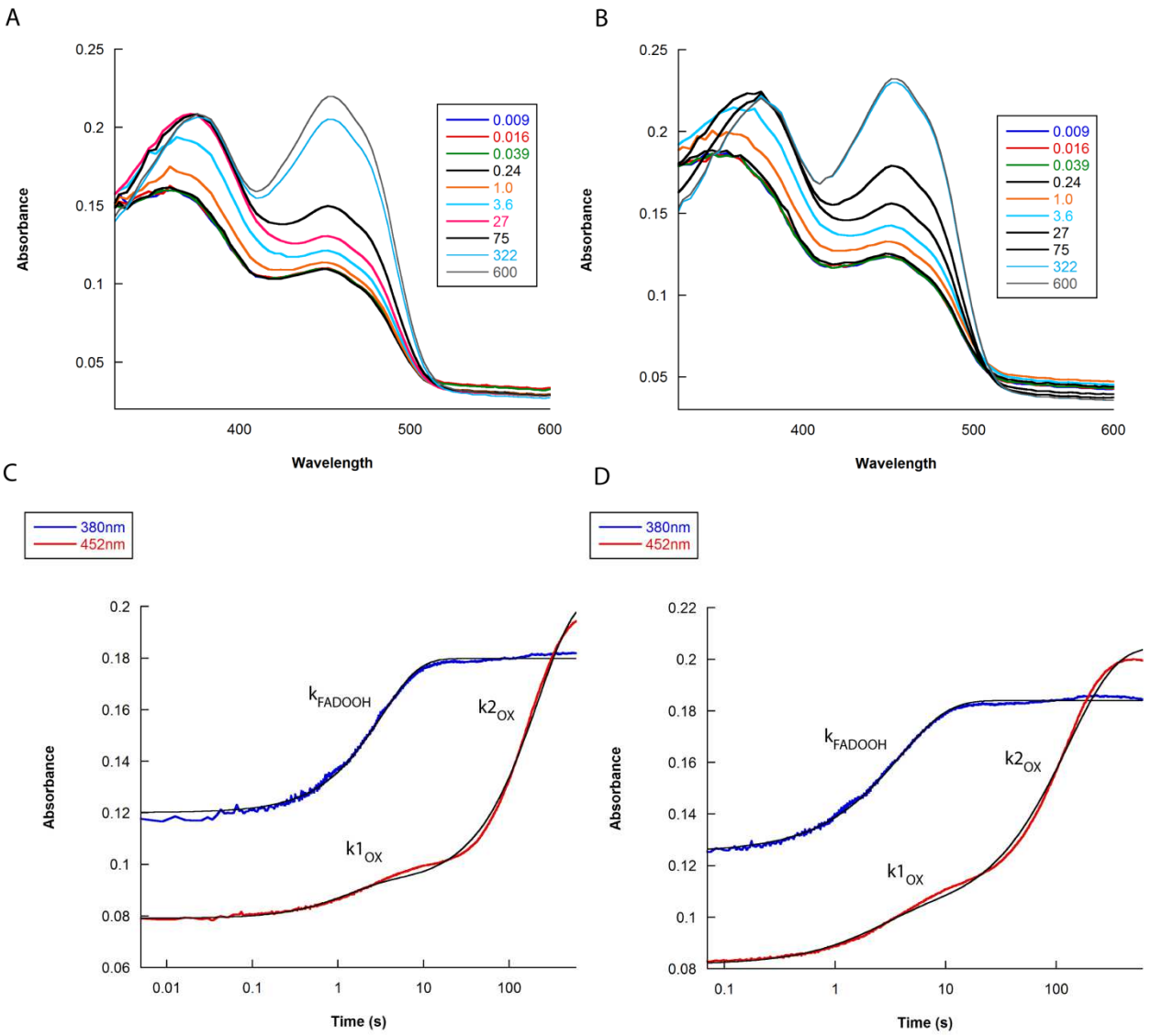

Figure 3.13. The oxidative half reaction was measured for R279A mutant enzyme. The top panels are traces of the oxidative half reaction for R279A at various time points with A) NADPH and B) NADH. The bottom panels follow the absorbance at 380 nm and 452 nm with C) NADPH and D) NADH. The fits shown in panels C and D are outlined by a thin black line and were fit to either single or double exponential growth or decay. The X axis is displayed in the logarithmic time scale to more clearly visualize the data.

Table 3.6. The kinetic values for the oxidative half reaction for WT enzyme are listed here as determined from the plots in figure 3.12.

	NADPH			NADH		
Enzyme	$k1_{FADOOH}$ (s^{-1})	$k2_{FADOOH}$ (s^{-1})	$k1_{OX}$ (s^{-1})	$k2_{ox}$ (s^{-1})	k_{FADOOH} (s^{-1})	k_{OX} (s^{-1})
WT	0.22 ± 0.001	0.005 ±0.0001	0.158 ± 0.002	0.008 ± 0.0001	0.131 ± 0.001	0.011 ± 0.0001

Table 3.7. The kinetic values for the oxidative half reaction for R279A are listed here as determined from the plots in figure 3.13.

	NADPH			NADH		
Enzyme	k_{FADOOH} (s^{-1})	$k1_{OX}$ (s^{-1})	$k2_{OX}$ (s^{-1})	k_{FADOOH} (s^{-1})	$k1_{OX}$ (s^{-1})	$k2_{OX}$ (s^{-1})
R279A	0.310± 0.002	0.816 ±0.04	0.005 ± 0.0001	0.258 ± 0.001	0.443 ± 0.014	0.008 ± 0.0002

c. Kinetic characterization of WT and Arg279A with the allosteric effector L-arginine

A paper was recently published describing L-arginine as an allosteric activator of SidA [12]. In order to understand this effect in a more complete sense, we characterized WT kinetics in the presence of L-arginine. L-arginine is involved in the biosythesis of L-ornithine making it likely that L-arginine can have an allosteric effect on this L-ornithine hydroxylase.

The kinetics of the WT enzyme were first analyzed by measuring oxygen consumption and product formation at steady state. The addition of L-arginine increases oxygen consumption by 58%. Additionally, this change is reflected in the hydroxylation assay. The oxidase activity of this enzyme was measured by measuring oxygen consumption in the absence of substrate. The measured rate corresponds to the slow re-oxidation of the flavin. In the absence of substrate a rate of $0.05s^{-1}$ was measured; however, when L-arginine is added this rate slows to $0.02s^{-1}$. This change suggests that L-arginine does not act to uncouple the enzyme like L-lysine, but instead improves the stability of the hydroperoxyflavin intermediate (Table 3.8).

Table 3.8. A comprehensive list of steady state kinetic values for WT enzyme are shown here.

Substrate	k_{cat} (s^{-1})	K_M (mM)	% Coupling
NADPH[1]	0.45 ± 0.01	0.007 ± 0.001	92
NADPH + 1 mM Arg[1]	0.73 ± 0.03	0.007 ± 0.003	97
L-ornithine[2]	0.46 ± 0.02	0.645 ± 0.011	89
L-lysine[2]	0.17 ± 0.01	0.680 ± 0.012	16
L-ornithine + 1 mM L-Arg[2]	0.71 ± 0.02	1.2 ± 0.14	97
None (oxidase act)	0.05 ± 0.01	-	-
L-Arginine	0.02 ± 0.01	-	-

[1][L-ornithine] was kept constant at 10 mM, the K_M given is for NADPH
[2][NADPH] was kept constant at 1 mM, the K_M given is for L-ornithine/ L-lysine

We were able to measure a K_M of activation (K_A) for the enzyme by incubating a saturated reaction mixture with various concentrations of L-arginine. A K_A of 60 μM was measured with the coenzyme NADPH and a K_A of 550 μM was measured for NADH. The difference between K_A values between coenzymes is roughly 10 fold, exactly the same fold change measured for the K_M values of NADPH and NADH (Figure 3.14, Table 3.9). This strongly suggests that an enzyme/coenzyme/activator complex is formed in order to achieve maximal activation of SidA. The same analysis was done using the R279A mutant. We measured a K_A for L-arginine with NADPH of 2 mM for the mutant enzyme. This roughly 40 fold difference is exactly the same fold change observed when comparing K_M values for NADPH between mutant and WT enzyme. This supports the observation that an enzyme/coenzyme/activator complex is formed.

Using the information from these experiments, we measured product formation at saturating concentrations of L-arginine. The rate of hydroxylation showed a significant increase only when the enzyme was reduced with NADPH. There was little to no change in product formation when the coenzyme NADH was used for both WT and mutant enzyme. Thus, the changes seen in oxygen consumption with NADH are due to uncoupling of the enzyme leading to production of H_2O_2. This data clearly shows that the activating effect of L-arginine is dependent on the 2'phosphate (Figure 3.15, Table 3.10). It is unclear; however if the 2'phosphate is interacting directly with the activator to improve enzyme function.

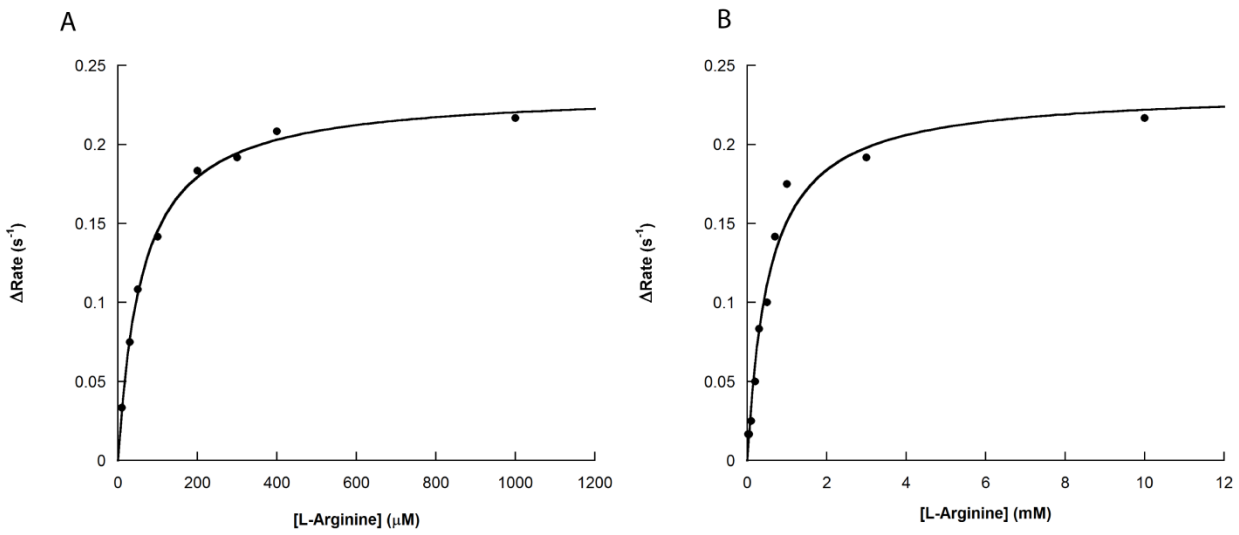

Figure 3.14. The rate of oxygen consumption for WT and R279A is enhanced with the addition of L-arginine. Each assay was done in the presence of 15 mM L-ornithine, 1 and 3 mM NADPH for WT and R279A respectively, and 2 μM final enzyme concentration in a 1 mL total reaction volume with the addition of varying [L-arginine]. ΔRates were obtained by subtracting out the rate of reaction in the absence of L-arginine.

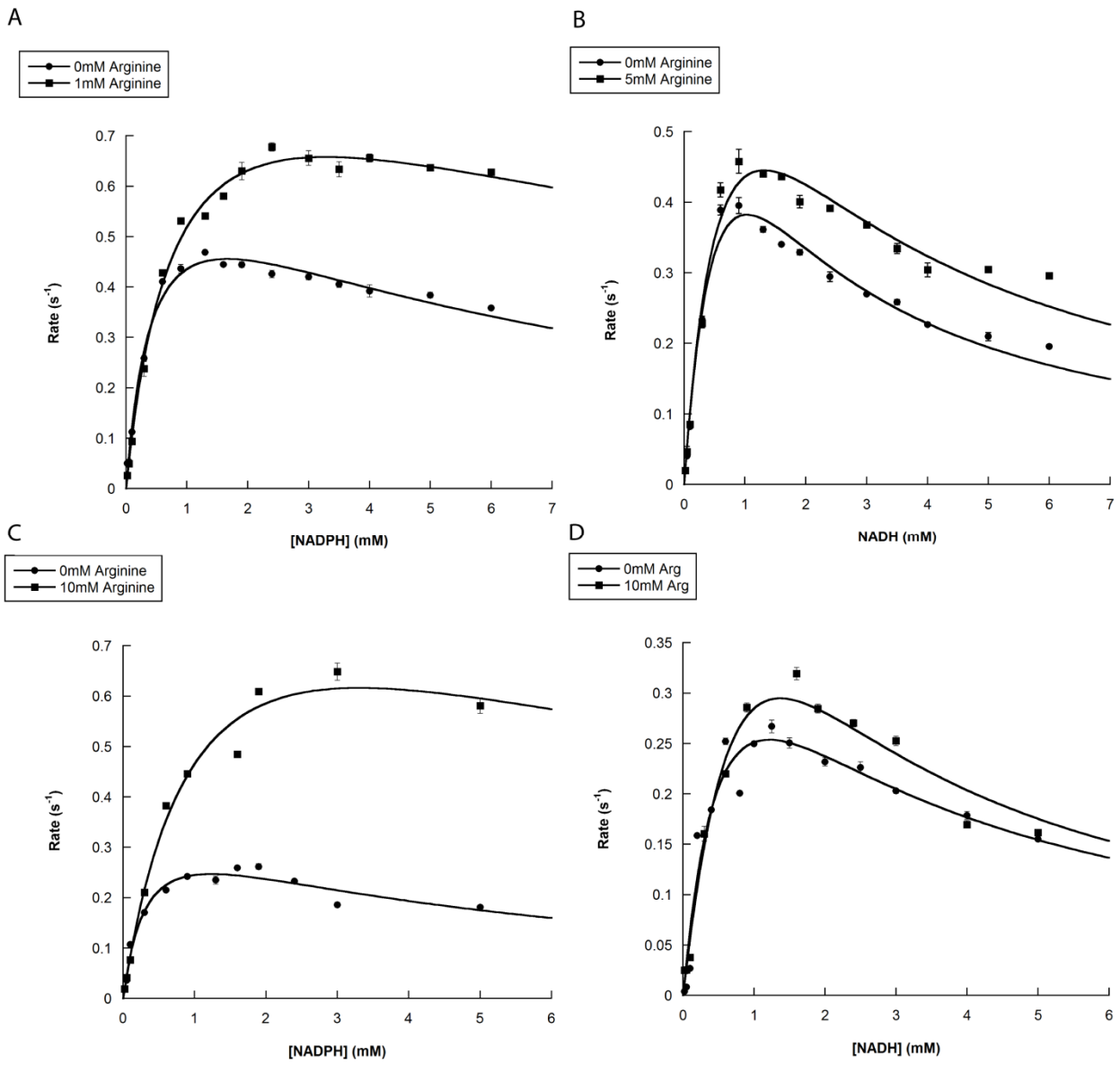

Figure 3.15. The rate of N^5-hydroxyornithine formation is enhanced by the addition of L-arginine WT and R279A with NADPH. Product formation for WT enzyme is shown in panels A) NADPH and B) NADH. Product formation for R279A is shown in panels C) NADPH and D) NADH. Assays were done using 15 mM L-ornithine and saturating concentrations of L-arginine as determined by the oxygen consumption assay.

Table 3.9. L-arginine enhances oxygen consumption for WT and R279A.

	NADPH		NADH	
Enzyme	k_{act} (s^{-1})	K_A (mM)	k_{act} (s^{-1})	K_A (mM)
WT	0.23 ± 0.01	0.060 ± 0.001	0.23 ± 0.02	0.55 ± 0.08
R279A	0.38 ± 0.01	2.0 ± 0.26	0.41 ± 0.01	1.1 ± 0.12

Table 3.10. L-arginine enhances the rate of N^5-hydroxyornithine formation with NAD(P)H for WT and R279A.

	NADPH			NADH		
Enzyme + L-arginine	k_{cat} (s^{-1})	K_M (mM)	K_i (mM)	k_{cat} (s^{-1})	K_M (mM)	K_i (mM)
WT	1.0 ± 0.05	0.84 ± 0.13	12.9 ± 3.0	1.0 ± 0.2	0.8 ± 0.2	2.1 ± 0.6
R279A	1.03 ± 0.1	1.1 ± 0.4	9.8 ± 3	0.7 ± 0.1	0.6 ± 0.3	2 ± 1

In order to further understand the role of L-arginine, the reductive and oxidative half reactions were probed using the stop flow. The reductive half reaction was probed by incubating enzyme with 1 mM NADPH and various concentrations of L-arginine. The K_A values measured for L-arginine differed from the K_A values determined from those at steady state for the WT enzyme. A K_A for L-arginine of 650 μM was measured for WT, and a K_A for L-arginine of 1.95 mM was measured for R279A. At saturating concentrations of L-arginine, k_{red} increased 6 fold for WT enzyme and 8 fold for R279A mutant enzyme (Figure 3.16, Table 3.11). Although, the rate of reduction is influenced very heavily by the addition of L-arginine, there is a much smaller effect at steady state suggesting that when L-arginine is present, flavin reduction is no longer the rate limiting step of the reaction.

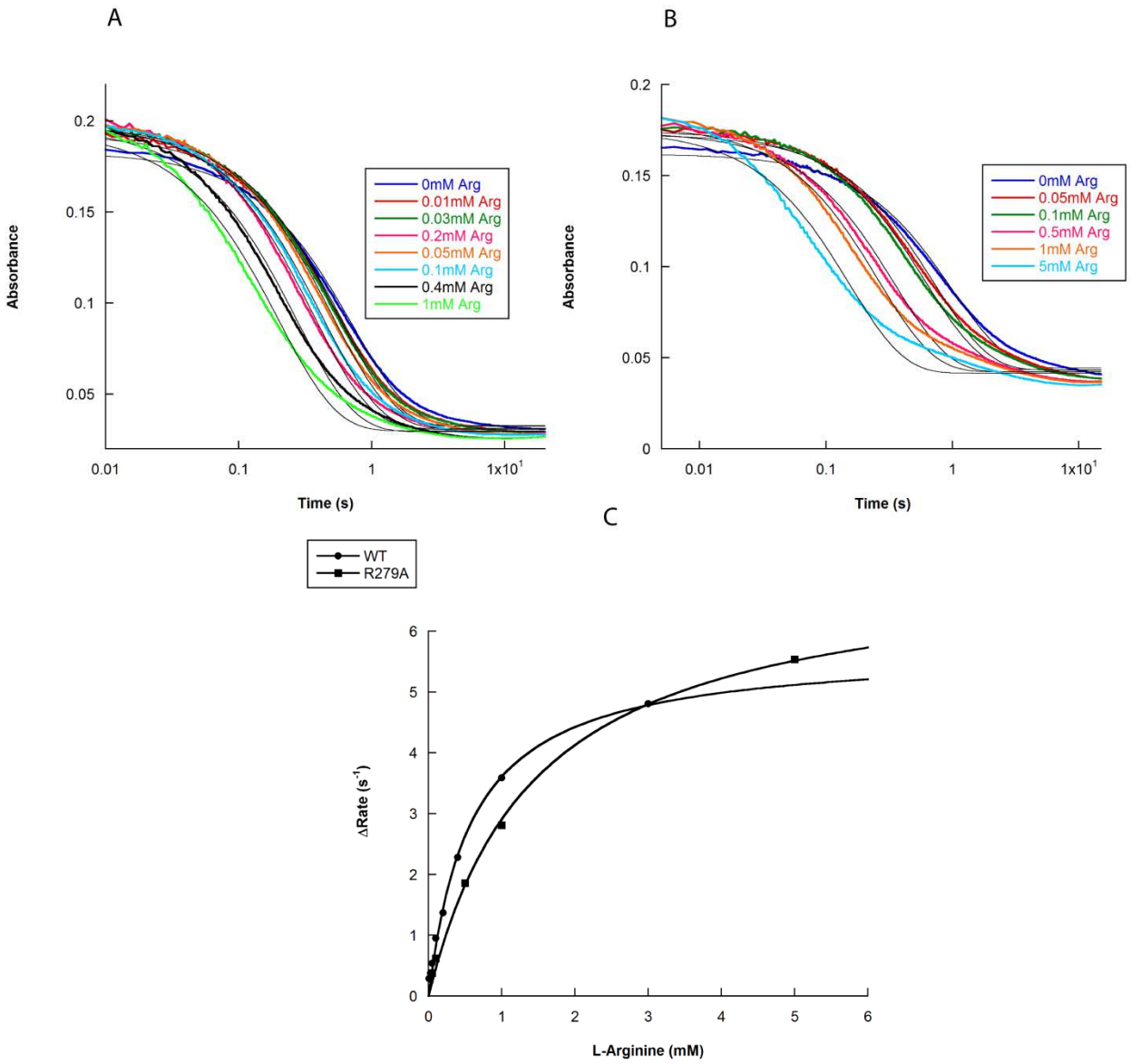

Figure 3.16. The rate of the reductive half reaction is enhanced for WT and R279A mutant enzyme by L-arginine. Panel A and B show traces of the reductive half reaction for A) WT and B) R279A with the addition of L-arginine at various concentrations. Panel C shows the plot of the absorbance at 452 nm. The fits for each individual reductive half reaction in panels A and B are outlined by a thin black line and were plotted to a single exponential decay.

Table 3.11. The values for the rate enhancement observed in the reductive half reaction with L-arginine are shown here.

	NADPH	
Enzyme	k_{act} (s^{-1})	K_A (mM)
WT	6.03 ± 0.11	0.657 ± 0.046
R279A	8.17 ± 0.33	1.95 ± 0.26

Data regarding the oxidative half reaction is incomplete for the R279A mutant but WT data with NADPH has recently been completed. L-arginine enhances the rate of formation of the C4a-hydroperoxyflavin adduct over 50 fold and increases the stability of the intermediate as well. At 200μM O_2, the formation of the intermediate (FAD_{OOH}) increases from $0.22s^{-1}$ to $11.1s^{-1}$ in the presence of saturating L-arginine. It is interesting to note that a second phase is not observed when measuring A_{380}; however it is possible that the rate corresponding to the decay of the C4a-hydroperoxyflavin is too slow to measure. In the absence of L-arginine, re-oxidation of the flavin begins to occur after 15 s while in the presence of L-arginine re-oxidation of the flavin begins after 50 s (Figure 3.17). When L-arginine is present, the rate of $k1_{OX}$ is significantly faster changing from $0.158s^{-1}$ to $8.62s^{-1}$. This roughly 50 fold increase in rate provides evidence that $k1_{OX}$ corresponds to the formation of the intermediate which is greatly enhanced by the presence of L-arginine. The rate of re-oxidation of the flavin ($k2_{OX}$) in the absence of L-arginine is $0.008s^{-1}$ but in the presence of L-arginine FAD_{OX} is $0.005s^{-1}$ (Table 3.5, Table 3.12). From this data it is clear that L-arginine not only acts to improve the rate of reduction but enhance the formation and stability of the critical intermediate the C4a-hydroperoxyflavin.

The effect of L-arginine on the oxidative half reaction is similar with NADH. Formation of the C4a-hydroperoxyflavin is improved as well as stability. $k1_{FADOOH}$ changes from $0.131s^{-1}$ to $2.46s^{-1}$ with the addition of L-arginine, a 19 fold increase (Table 3.5, Table 3.12). Additionally, a second phase appears, $k2_{FADOOH,}$ which corresponds to decay of the C4a-hydroperoxyflavin indicating that addition of L-arginine allows the intermediate to persist long enough to measure the decay unlike in its absence. When measuring the absorbance at 452nm, 2 phases were observed, $k1_{OX}$ corresponds to the formation of the C4a-hydroperoxyflavin intermediate as previously discussed which was not apparent in the absence of L-arginine. $k2_{OX}$ was very similar

to those values obtained for the WT enzyme in the absence of L-arginine suggesting strongly that this rate corresponds to decay of the C4a-hydroperoxyflavin. These observations suggest that L-arginine allows the enzyme to function more efficiently with NADH as well but does not achieve a maximal effect as seen with NADPH.

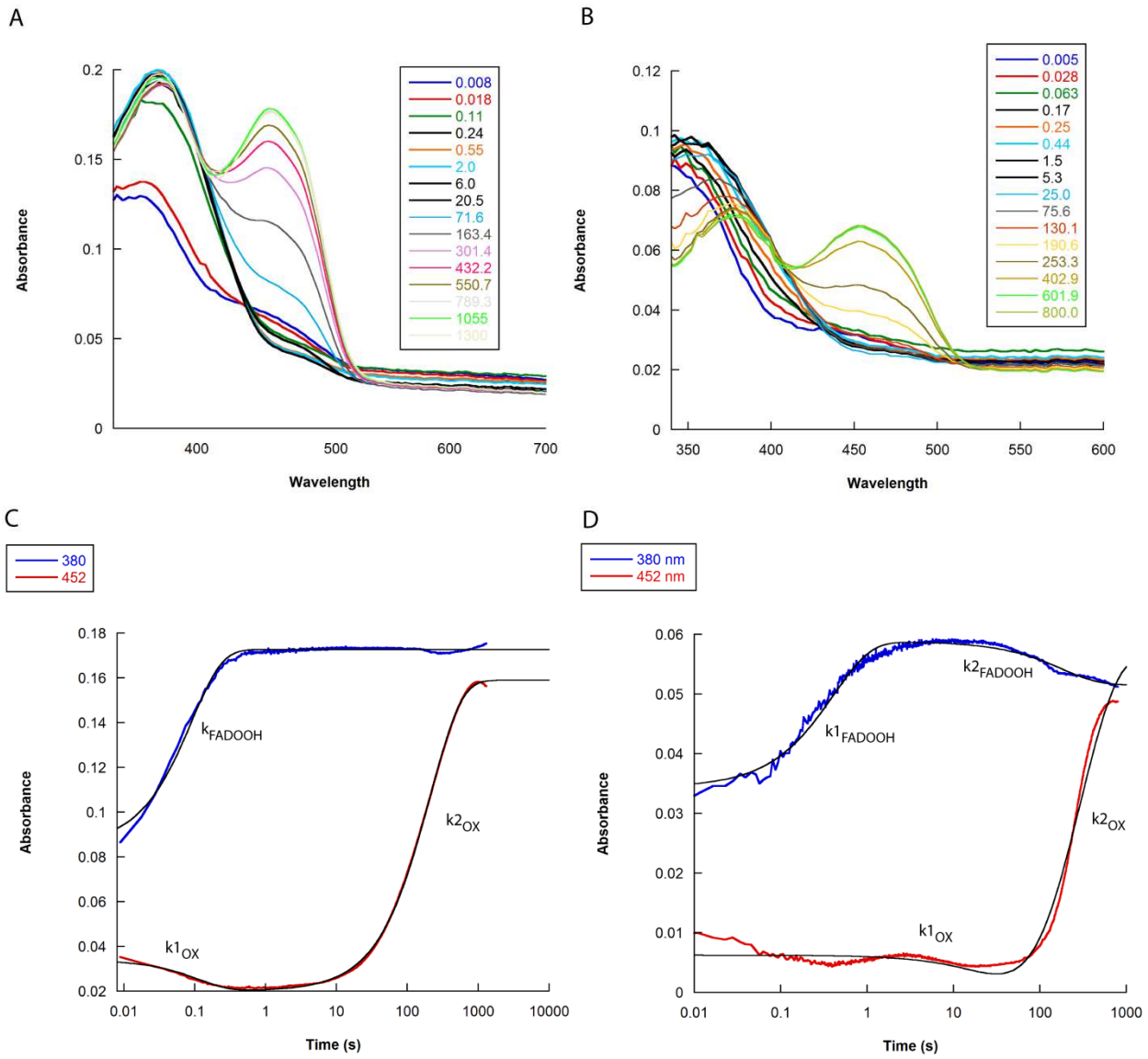

Figure 3.17. The oxidative half reaction is greatly affected by the addition of L-arginine. The top panels show the oxidative half reaction for WT enzyme with the addition of L-arginine at various times for A) NADPH and B) NADH. The bottom panels show plots of absorbance at 380 nm and 452 nm for the above traces for C) NADPH and D) NADH. The fits in panels C and D are outlined by a thin black line and were plot to either single or double exponential growth or decay.

Table 3.12. L-arginine significantly impacts the oxidative half reaction of WT enzyme with NADPH and NADH. These values were derived from figure 3.17.

	NADPH			NADH			
Enzyme	k_{FADOOH} (s^{-1})	$k1_{OX}$ (s^{-1})	$k2_{OX}$ (s^{-1})	$k1_{FADOOH}$ (s^{-1})	$k2_{FADOOH}$ (s-1)	$k1_{OX}$ (s^{-1})	$k2_{OX}$ (s^{-1})
WT + L-arginine	11.1 ± 0.13	8.62 ± 0.42	0.005 ± 0.0001	2.46 ± 0.03	0.006 ± 0.0002	0.025 ± 0.001	0.0035 ± 0.0001

CHAPTER IV

Conclusions

SidA is a highly specific L-ornithine hydroxylase that shows both a high specificity for L-ornithine and for the coenzyme NADPH. In order to design an effective inhibitor, we needed to develop a complete understanding of this enzyme and mechanism through structural and mutational analysis. The structure of SidA in complex with L-ornithine and L-lysine allowed us to speculate that SidA controls its amino acid selectivity by distance to the C4a-hydroperoxyflavin intermediate. Additionally, the reduced structures contained L-OrnOH allowing us to determine that SidA is active in crystal form. This means that the C4a-hydroperoxyflavin intermediate can be formed in the crystal and this intermediate may be able to be observed in a crystal structure.

The crystal structure of SidA showed that, Arg279 interacts with the 2'phosphate specific to $NADP^+$ as well as the adenine moeity of this molecule. We speculated that this interaction is critical to selectivity for NADP(H) over NAD(H). We also speculated that the interactions with the adenine moeity would be important for tight binding of the coenzyme and possibly influence stability of the intermediate. The Arg279A mutant was critical in testing this hypothesis. This mutant showed little difference in oxygen reactivity; however, K_M values for both coenzymes became much more similar. We speculate that the lack of specificity observed is due to interactions with the 2'phosphate. Additionally, the K_M values for both coenzymes increased well above WT levels suggesting that the interaction with the adenine moeity is equally critical. The substrate hydroxylation assay showed us that although levels of oxygen consumption were about equal, the amount of product formation was significantly less for the mutant. The observed

uncoupling with both coenzymes tells us that the interaction with the adenine moeity is very important in stabilizing the C4a-hydroperoxyflavin intermediate.

As expected, the reductive half reaction supported our hypothesis showing little to no specificity for coenzymes as well as a higher binding affininty. The oxidative half reaction was of particular interest showing a completely different profile for re-oxidation of the flavin. The re-oxidation in the R279A mutant occurred in positive phases. The first phase was a rapid decay of the C4a-hydroperoxyflavin, where as in the WT enzyme this rate was slower with a negative absorbance. The second phase proceded with a rate equivelent to that of WT enzyme and corresponded to the decay of the C4a-hydroperoxyflavin. Experiments done with NADH were quite similar showing an almost identical profile for R279A which lacks specificty for coenzymes. The oxidative half reaction for WT enzyme with NADH showed only two phases revelaing that the 2'phosphate specific to NADPH is essential for proper intermediate stabilization. Again, the extremely poor stability observed in the R279A mutant is likely due to a combination of losing the interaction with the 2'phosphate as well as with the adenine moiety.

The effect of L-arginine on the WT and R279A mutant enzyme gave insight into the mechanism of oxygen activation and substrate hydroxylation of this enzyme. A significant increase in oxygen consumption was observed for both WT and R279A mutant when L-arginine was added. This increase in oxygen activation only translated to an increase in product formation when reducing the enzyme with NADPH. When reduced with NADH, the reaction became more uncoupled. It is clear from the K_A values obtained by comparing R279A and WT that an enzyme/$NADP^+$/ L-arginine complex is formed because the K_A values show very similar fold changes to those of NAD(P)H.

L-arginine effects both the oxdiative and reductive half reactions. Adding L-arginine is able to increase the rate of reduction by 6 fold for WT enzyme and 8 fold for the R279A mutant enzyme. The rate of reduction is the rate limmiting step of the hydroxylation reaction. This improvement in the rate of reduction most likely accounts for the increase in steady state values; however, it is clear that there is another step in the reaction that proceeds with only a slightly faster rate than that of reduction since a <2 fold change is observed in the steady state. The oxidative half reaction shows that the addition of L-arginine causes the C4a-hydroperoxyflavin intermediate to form roughly 50 fold faster than in the absence of substrate, while improving the stability of the intermediate.

The structure of the SidA co-crystallized with $NADP^+$ and L-arginine showed an arginine bound in the active site and in another site capable of interacting with the adenine ring of NADP. We believe that the binding of L-arginine in the active site is the cause for the observed allosteric enhancment of this enzyme as it has been shown that a postive charge near the flavin improves oxygen activation.

The work to crystallize this enzyme and understand substrate selectivity for both L-ornithine and NADPH will hopefully prove important in designing inhibitors that are specific and effective against SidA. Additionally, this information is important in understanding oxygen activation by flavin containing monooxygenases and more specifically NMOs. The residue Arg279 which was a primary focus of this thesis is highly conserved in many flavin containing monooxygenases that preferntially utilitze NADPH. Thus, the information may be quite relevant all NADPH dependent FMOs.

REFERENCE LIST

1. Abad, A., et al., *What makes Aspergillus fumigatus a successful pathogen? Genes and molecules involved in invasive aspergillosis.* Rev Iberoam Micol, 2010. **27**(4): p. 155-82.
2. Horn, F., et al., *Systems biology of fungal infection.* Front Microbiol, 2012. **3**: p. 108.
3. Knutsen, A.P. and R.G. Slavin, *Allergic bronchopulmonary aspergillosis in asthma and cystic fibrosis.* Clin Dev Immunol, 2011. **2011**: p. 843763.
4. Knutsen, A.P., et al., *Fungi and allergic lower respiratory tract diseases.* J Allergy Clin Immunol, 2012. **129**(2): p. 280-91; quiz 292-3.
5. He, H., et al., *Clinical features of invasive bronchial-pulmonary aspergillosis in critically ill patients with chronic obstructive respiratory diseases: a prospective study.* Crit Care, 2011. **15**(1): p. R5.
6. Nevitt, T., *War-Fe-re: iron at the core of fungal virulence and host immunity.* Biometals, 2011. **24**(3): p. 547-58.
7. Haas, H., *Iron - A Key Nexus in the Virulence of Aspergillus fumigatus.* Front Microbiol, 2012. **3**: p. 28.
8. Wallner, A., et al., *Ferricrocin, a siderophore involved in intra- and transcellular iron distribution in Aspergillus fumigatus.* Appl Environ Microbiol, 2009. **75**(12): p. 4194-6.
9. Chocklett, S.W. and P. Sobrado, *Aspergillus fumigatus SidA is a highly specific ornithine hydroxylase with bound flavin cofactor.* Biochemistry, 2010. **49**(31): p. 6777-83.
10. Romero, E., et al., *Dual role of NADP(H) in the reaction of a flavin dependent N-hydroxylating monooxygenase.* Biochim Biophys Acta, 2012. **1824**(6): p. 850-7.

11. Robinson, R. and P. Sobrado, *Substrate binding modulates the activity of Mycobacterium smegmatis G, a flavin-dependent monooxygenase involved in the biosynthesis of hydroxamate-containing siderophores.* Biochemistry, 2011. **50**(39): p. 8489-96.

12. Frederick, R.E., J.A. Mayfield, and J.L. DuBois, *Regulated O2 activation in flavin-dependent monooxygenases.* J Am Chem Soc, 2011. **133**(32): p. 12338-41.